The Canadian Mineralogist
Vol. 43, pp. 409-442 (2005)

TECTONOMETAMORPHISM AT *ca.* 2.35 AND 1.85 Ga IN THE RAE DOMAIN, WESTERN CHURCHILL PROVINCE, NUNAVUT, CANADA: INSIGHTS FROM STRUCTURAL, METAMORPHIC AND *IN SITU* GEOCHRONOLOGICAL ANALYSIS OF THE SOUTHWESTERN COMMITTEE BAY BELT

Robert G. BERMAN[§], Mary SANBORN-BARRIE, Richard A. STERN[¶] and Chris J. CARSON[‡]

Continental Geoscience Division, Geological Survey of Canada, 615 Booth Street, Ottawa, Ontario K1A 0E9, Canada

Abstract

New constraints on the Paleoproterozoic evolution of the Rae domain, western Churchill Province, Nunavut, are provided through a linked structural, metamorphic, and *in situ* geochronological investigation of the southwestern part of the Archean Committee Bay belt. Within D_2 strain shadows proximal to a *ca.* 2.72 Ga synvolcanic pluton, S_1 is recognized as a northward-striking, east-dipping foliation associated with west-vergent D_1 folds and possible thrusts. The D_1 structures are variably overprinted by a northeast-striking, southeast-dipping S_2 foliation associated with shallowly northeast-plunging, northwest-vergent F_2 folds. Whereas some textural observations suggest a cryptic, pre-D_1 thermal event that may be related to widespread *ca.* 2.61–2.58 Ga granitic plutonism, porphyroblast–fabric relationships in metapelitic rocks demonstrate that two main metamorphic events occurred, syn- to post-D_1 (M_1) and syn- to post-D_2 (M_2). Thermobarometric data and quantitative phase diagrams indicate relatively low-*P*, clockwise *P–T*–t paths culminating in post-tectonic growth of andalusite during both M_1 and M_2. Monazite inclusions in late- to post-D_1 garnet and staurolite yield a 2344 ± 6 Ma age population that, on the basis of microtextural features, effectively dates M_1 metamorphism at a late stage of D_1 strain. Monazite growth occurred between 520 and 560°C. Event M_2 is dated by matrix monazite that forms a 1838 ± 5 Ma age population. The absence of magmatic rocks of appropriate age that could provide heat, together with clockwise *P–T*–t paths and porphyroblast growth at a late stage of both D_1 and D_2 contractional strain events, collectively point to metamorphism as a consequence of crustal shortening and thickening. The compressional forces that drove modest thickening events across the Committee Bay belt at *ca.* 2.35 and 1.85 Ga (average belt-wide ages) are considered to reflect far-field, upper-plate reworking during two orogenic events. The first event may have involved *ca.* 2.35 Ga collisional orogenesis (the "Arrowsmith" orogeny) following a period of continental arc magmatism on the western Rae margin. The second event is considered to be related to an early accretionary stage of the Trans-Hudson orogeny involving *ca.* 1.88–1.86 Ga collision of microcontinents located in the vicinity of Hudson Bay.

Keywords: metamorphism, tectonics, geochronology, monazite, western Churchill Province, SHRIMP, thermobarometry, Committee Bay, Rae domain, Arrowsmith orogeny, Nunavut.

Sommaire

De nouvelles contraintes sont maintenant disponibles pour élucider l'évolution paléoproterozoïque du domaine Rae, dans le secteur ouest de la Province de Churchill, au Nunavut; on se sert d'études intégrées des aspects structuraux, métamorphiques et géochronologiques, ces derniers établis *in situ*, du secteur sud-ouest de la ceinture archéenne de Committee Bay. Au sein des zones protégées de la déformation D_2 voisines d'un pluton synvolcanique d'environ 2.72 Ga, nous avons établi que la foliation S_1 est orientée vers le nord, à pendage vers l'ouest, en association avec des plis D_1 et possiblement des chevauchements dirigés vers l'ouest. Les structures D_1 sont partiellement oblitérées par une foliation S_2 orientée vers le nord-est, à pendage vers le sud-est, en association avec des plis F_2 à plongement axial légèrement vers le nord-est et indiquant une contraction vers le nord-ouest. Quoique certaines observations texturales font penser à un événement thermique cryptique pré-D_1 qui pourrait résulter d'un plutonisme granitique répandu à environ 2.61–2.58 Ga, les relations entre porphyroblastes et leurs matrices dans les roches métapélitiques démontrent bien que deux événements principaux ont eu lieu, d'abord avec et suivant D_1 (M_1), et ensuite avec et suivant D_2 (M_2). Les données thermobarométriques et l'utilisation de diagrammes de phase quantitatifs indiquent des tracés d'évolution métamorphiques *P–T*–t à faible pression, dans le sens de l'horloge, pour atteindre une croissance post-tectonique de l'andalousite pendant M_1 et pendant M_2. Les inclusions de monazite dans le grenat et la staurolite tardifs ou postérieurs par rapport à D_1 mènent à une population d'âges de 2344 ± 6 Ma; à la lumière des microtextures, nous attribuons cet intervalle d'âge

§ *E-mail address*: rberman@nrcan.gc.ca
¶ *Present address*: University of Western Australia, 35 Stirling Highway, Crawley, WA 6009, Australia.
‡ *Present address*: Northern Territory Geological Survey, GPO 3000, Darwin, NT 0801, Australia.

à l'événement M_1, développé à un stade tardif de la déformation D_1. La croissance de la monazite a eu lieu entre 520 et 560°C. L'âge de l'événement M_2 est fixé par l'âge de la monazite dans la matrice, qui donne 1838 ± 5 Ma. D'après l'absence de roches magmatiques d'âge approprié pouvant fournir la chaleur nécessaire, les tracés *P–T*–t dans le sens de l'horloge, et la croissance tardive de porphyroblastes associés aux deux événements de déformation contractionnelle, D_1 et D_2, le métamorphisme était une réponse à la contraction et l'épaississement de la croûte. Les forces de compression qui ont causé ces événements d'épaississement de part et d'autre de la ceinture de Committee Bay à environ 2.35 et 1.85 Ga, *grosso modo*, seraient des effets à distance dans la plaque supérieure de deux événements orogéniques. Le premier (l'orogenèse "Arrowsmith") pourrait témoigner d'une collision à environ 2.35 Ga postérieure à une période de magmatisme dans un arc continental le long de la bordure ouest de la ceinture de Rae. Le second serait lié à une accrétion précoce au cours de l'orogenèse trans-hudsonnienne impliquant une collision à environ 1.88–1.86 Ga de microcontinents dans la région de la baie d'Hudson.

(Traduit par la Rédaction)

Mots-clés: métamorphisme tectonique, géochronologie, monazite, Province de Churchill (secteur ouest), datations SHRIMP, thermobarométrie, Committee Bay, domaine de Rae, orogenèse Arrowsmith, Nunavut.

Introduction

Deciphering the history of polymetamorphic rocks is a particularly challenging endeavor facing metamorphic petrologists. As a first-order difficulty, complex textures that may be recorded during prograde, peak, and retrograde metamorphism on a single *P–T*–t path are generally difficult to distinguish from textural relationships produced during multiple metamorphic events (*e.g.*, Argles *et al.* 1999). These textural ambiguities have recently become tractable with the development of geochronological techniques capable of dating the growth of refractory porphyroblasts that have the potential to survive subsequent reworking (*e.g.*, Cohen *et al.* 1988, Christensen *et al.* 1989, Vance & O'Nions 1990, 1992, Burton & O'Nions 1991, DeWolf *et al.* 1993, Lanzirotti & Hanson 1995, Frei *et al.* 1995, Zhu *et al.* 1997, Vance *et al.* 1998b, Argles *et al.* 1999, Vance & Harris 1999, Foster *et al.* 2000, Prince *et al.* 2000, Stern & Berman 2000, Jung & Mezger 2001). In addition to providing the critical temporal link to quantitative metamorphic constraints (*e.g.*, Mezger *et al.* 1989, Frei *et al.* 1995, Vance *et al.* 1998b, Vance & Harris 1999, Berman *et al.* 2000a), these techniques also provide the means for determining the age of tectonic fabrics that bear specific relationships to dated porphyroblasts (Berman *et al.* 2000a, Stern & Berman 2000, Williams & Jercinovic 2002, Carson *et al.* 2004).

In this paper, we utilize *in situ* SHRIMP dating of monazite-(Ce) (henceforth referred to as simply monazite), together with structural and quantitative metamorphic data, to elucidate the tectonothermal history of a portion of the Rae domain that extends west from Committee Bay, Nunavut. This study represents part of an ongoing project aimed at understanding the polymetamorphic history of the western Churchill Province *via* a combination of *in situ* geochronological and petrological studies of metamorphic rocks. Previous work in the northwestern Hearne subdomain (Fig. 1) has documented metamorphic events at 2.56–2.50, 1.90–1.89, 1.85–1.83, and 1.75 Ga that affected different crustal blocks with distinct low- and high-*P* histories (Berman *et al.* 2000a, 2002a, b, Stern & Berman 2000). Preliminary results of a similar study initiated in the northern Rae domain indicate that low-*P* metamorphic events at 2.35, 1.85, and 1.78 Ga affected the highest grade, northern part of the Committee Bay belt (Carson *et al.* 2002, 2004, Berman *et al.* 2003). The latter dataset provides compelling constraints for a *ca.* 1.85 Ga (D_2) event, which was attributed to regional deformation related to hinterland reworking during an early (pre-terminal collision) stage of the Trans-Hudson orogeny. In the present contribution, we complement these initial findings by documenting new *in situ* geochronological data, as well as structural and metamorphic constraints from the lower-grade southwestern part of this belt. Our major focus is on unravelling the early (pre-D_2) structural and metamorphic history of this region from rocks that have been partially shielded from the effects of regional D_2 strain. Macroscopic and microscale data reported herein provide new insights into the early Paleoproterozoic, pre-Hudsonian evolution of the Committee Bay belt, with important implications for the tectonic evolution of the Rae domain.

Geological Setting

The western Churchill Province represents variably reworked Archean continental crust and Paleoproterozoic sedimentary cover that formed the upper plate hinterland to both the 2.0–1.9 Ga Thelon–Taltson orogen (Henderson *et al.* 1982, Hoffman 1988, Thériault 1992, Bostock & van Breemen 1994, McNicoll *et al.* 2000) to the west and the 1.9–1.8 Ga Trans-Hudson orogen (*e.g.*, Hoffman 1988, Ansdell *et al.* 1995, St-Onge *et al.* 2002) to the southeast (Fig. 1). The province is divided by the geophysically defined Snowbird tectonic zone (Gibb & Walcott 1971, Hoffman 1988, 1990) into the Rae and Hearne domains, both comprising attenuated, largely greenschist- to amphibolite-facies, *ca.* 2.72–2.68 Ga belts of supracrustal rocks intruded by *ca.* 2.7–2.6 Ga felsic plutons. A distinguishing feature of the Rae domain (Fig. 1) is the occurrence of greenstone belts that include komatiitic flows and associated chromian-muscovite-bearing quartzite. Correlative rocks are considered to extend over 1000 km from Baker Lake (Woodburn group: Ashton 1981, Fraser 1988) to Baffin Island (Mary River Group, Jackson 1966, 2000), and include the Prince Albert Group (PAg: Heywood 1967, Frisch 1982, Schau 1982) that extends for approximately 300 km from the Amer fault zone (Tella & Heywood 1978) to the western shore of Committee Bay (Fig. 1). The Rae domain exhibits considerable evidence (U–Pb and Nd model ages) for Mesoarchean crust in regions such as the Queen Maud block of the northern Rae domain (Q and QM, Fig.1; Thériault *et al.* 1994), and the Beaverlodge (Bl, Fig. 1; van Schmus *et al.* 1986) and Western Granulite domains (W, Fig. 1; Crocker *et al.* 1993) of northwestern Saskatchewan. The northwestern Hearne subdomain includes subvolcanic tonalite plutons and mafic-rock-dominated volcanic belts with local isotopic evidence for assimilation and clastic input of Mesoarchean crust (Sandeman *et al.* 2000). These rocks were intruded by *ca.* 2.6 Ga granitic plutons (Davis *et al.* 2000), and subjected to 2.56–2.50 Ga high-grade metamorphism and deformation (MacLachlan *et al.* 1999, Berman *et al.* 2000a, Stern & Berman 2000). In contrast, the central Hearne subdomain comprises juvenile, mafic and felsic, mixed tholeiitic and calc-alkaline volcanic belts that are cut by syn- to late-orogenic 2.68–2.65 Ga plutonic rocks (Davis *et al.* 2000).

Four Paleoproterozoic granitic suites are of regional importance (Fig. 1). The Thelon tectonic zone and Taltson magmatic zone comprise a 2.0–1.93 Ga calc-alkaline arc, and younger orogenic granitic batholiths in the western Rae domain (Henderson *et al.* 1999, Bostock & van Breemen 1994, McNicoll *et al.* 2000). Granitic rocks of *ca.* 1.87–1.85 Ga age include the Wathaman–Chipewyan (WB), Cumberland (CB), and Great Bear (GB) batholiths, considered to reflect continental arc magmatism produced by (in present-day coordinates) north-directed subduction (WB and CB) during the Trans-Hudson orogeny (Meyer *et al.* 1992, Thériault *et al.* 2001) and east-directed (GB) subduction during the Wopmay orogeny (Hoffman 1988). The *ca.* 1.85–1.81 Ga Hudson granites (Peterson *et al.* 2002), abundant throughout the Hearne and northeastern Rae domains (*e.g.*, Ford Lake batholith; LeCheminant *et al.* 1987), are interpreted to represent to orogenic lower crustal melts (Peterson *et al.* 2002). The *ca.* 1.76–1.75 Ga Nueltin granites, which straddle the central segment of the Snowbird tectonic zone, are considered to represent upper crustal melts triggered by a mafic underplate (Peterson *et al.* 2002).

Paleoproterozoic sedimentary rocks with significant areal extent in the western Churchill Province span a range of ages (Fig. 1). Erosional outliers of the Hurwitz Group (Bell 1970, Aspler & Chiarenzelli 1997) in the central Hearne subdomain consist of a 2.45 to 2.1 Ga lower sequence and a disconformable upper sequence with detrital zircon as young as 1.95–1.91 Ga (Davis *et al.* 2000, Aspler *et al.* 2001). Recent geochronological work (R.H. Rainbird & W.D. Davis, pers. commun., 2003) suggests that the upper Hurwitz Group is correlative with the Amer group of the Rae domain (Fig. 1). The *ca.* 1.85 – 1.79 Ga Baker Lake group may have formed in a transtensional, lateral escape basin during the Trans-Hudson orogeny (Rainbird *et al.* 2003) or in an extensional basin related to terminal collision or post-collisional processes of the Trans-Hudson orogen (Aspler *et al.* 2004). Subsequent thermal subsidence produced the large intracratonic, *ca.* 1.72 Ga Thelon and Athabasca basins (*e.g.*, Rainbird *et al.* 2003).

Geology of the Committee Bay Belt

Recent mapping of bedrock at a 1:100,000 scale (Committee Bay Targeted Geoscience Initiative) of three 1:250,000 mapsheets (Figs. 1, 2; from east to west: National Topographic System (NTS) sheets 56K, 56J-north/56O-south, 56P) in the Committee Bay region (Sandeman *et al.* 2001a, b, 2004, Sanborn-Barrie *et al.* 2002, 2003, Skulski *et al.* 2002a, 2003a, b), together with supporting geochronological investigations (summarized in Skulski *et al.* 2003b, with ages quoted below), have provided a geological framework for the present study. The Committee Bay belt (CBb) is broadly divided into three crustal subdomains, including (from north to south) the northern migmatite subdomain, the Prince Albert Group (PAg) subdomain, and the Walker Lake intrusive complex (Fig. 2; Skulski *et al.* 2003b). The central PAg subdomain is dominated by PAg supracrustal rocks, which attain a breadth of *ca.* 60 km in the southwest, proximal to a *ca.* 2.718 Ga synvolcanic tonalite, referred to here as the "Laughland Lake tonalite" (Fig. 2). To the northeast, the supracrustal belt is increasingly attenuated, and *ca.* 2.61–2.58 Ga felsic plutonic rocks that cut the PAg become more prevalent. Current constraints on the PAg indicate a lower volcanic-rock-dominated sequence of basalt, intercalated *ca.* 2.73 Ga felsic volcanic rocks, and a substantial (~300 m thick) komatiite sequence, overlain by a middle sedimentary-rock-dominated sequence of psammite, semipelite, and quartzite deposited between *ca.* 2.72 Ga (youngest detrital zircon in quartzite) and 2.71 Ga (age of conformably overlying intermediate tuff). The uppermost part of the PAg, deposited after *ca.* 2690 Ma, contains minor komatiite, iron formation, and clastic rocks. Oxide- and silicate-facies iron formation seems to have been deposited at two major stratigraphic horizons. The rocks are interpreted to reflect subaqueous hydrothermal systems active between, and after, *ca.* 2.73 and 2.71 Ga volcanic activity.

The southern Walker Lake intrusive complex is dominated by foliated, *ca.* 2.61 Ga magnetite-bearing, microcline augen granodiorite, with less voluminous, equigranular, *ca.* 1.82 Ga biotite ± fluorite monzo-

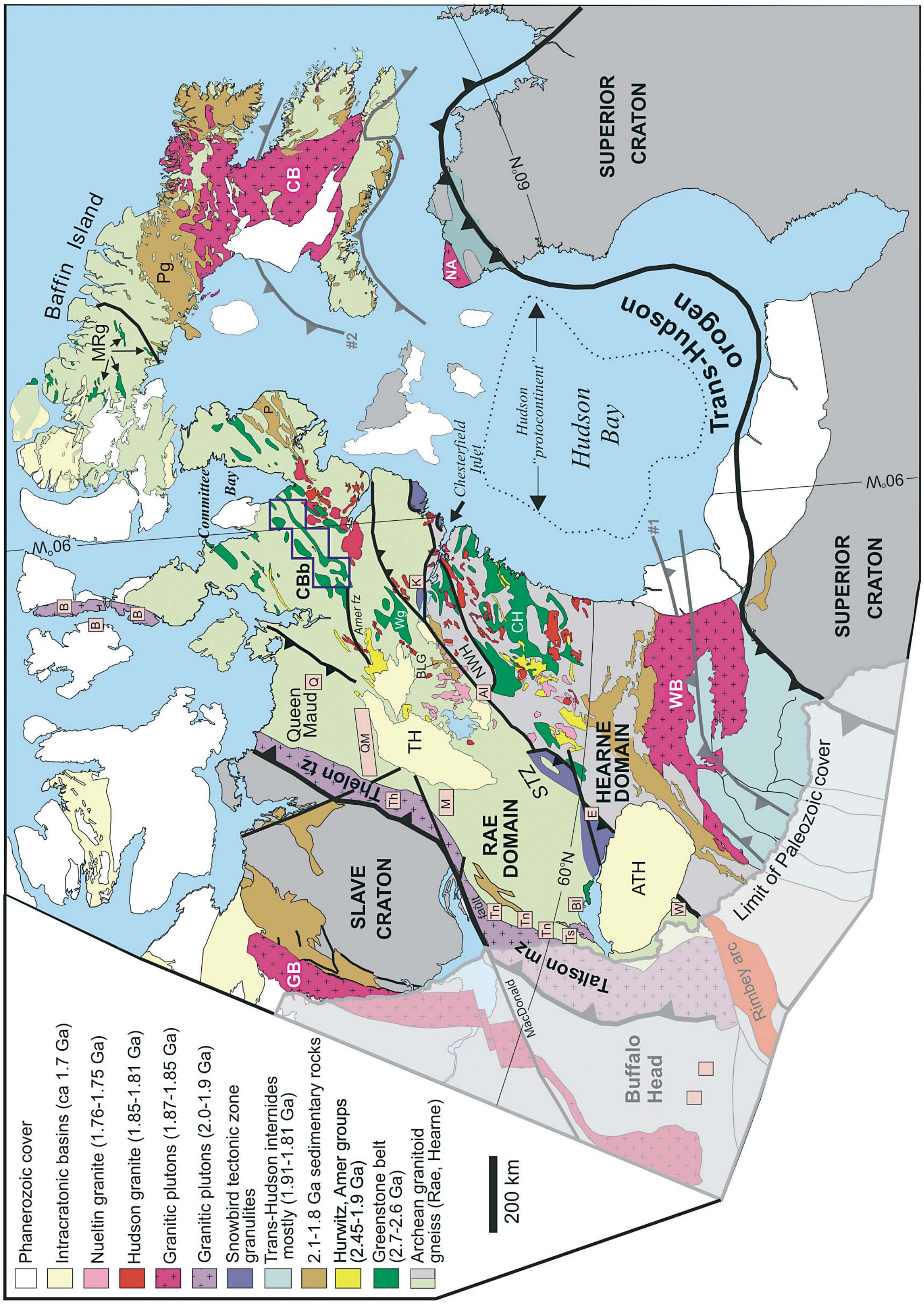

Phanerozoic cover
Intracratonic basins (ca 1.7 Ga)
Nueltin granite (1.76-1.75 Ga)
Hudson granite (1.85-1.81 Ga)
Granitic plutons (1.87-1.85 Ga)
Granitic plutons (2.0-1.9 Ga)
Snowbird tectonic zone granulites
Trans-Hudson internides mostly (1.91-1.81 Ga)
2.1-1.8 Ga sedimentary rocks
Hurwitz, Amer groups (2.45-1.9 Ga)
Greenstone belt (2.7-2.6 Ga)
Archean granitoid gneiss (Rae, Hearne)
200 km
Baffin Island
Pg
CB
MRg
#2
NA
SUPERIOR CRATON
60°N
Trans-Hudson orogen
Hudson Bay
Hudson "protocontinent"
Chesterfield Inlet
Committee Bay
90°W
CBb
Amer fz
Wg
CH
BLG
K
Al
Q
Queen Maud
QM
TH
Thelon tz
Th
M
RAE DOMAIN
STZ
HEARNE DOMAIN
WB
#1
E
ATH
SLAVE CRATON
GB
Taltson mz
Tn
Ts
Bl
W
MacDonald
Rimbey arc
Limit of Paleozoic cover
Buffalo Head

granite. The northern migmatite subdomain consists of migmatitic paragneiss, metatexite, diatexite, and associated garnet–biotite±sillimanite- and muscovite–biotite-bearing peraluminous granite, with metaluminous granodiorite plutons. The age of deposition of clastic rocks in the northern migmatite domain is bracketed between 2.69 ± 0.02 Ga, the age of the youngest detrital zircon in paleosome (Skulski *et al.* 2003b) and *ca.* 2.58 Ga, the U–Pb zircon age of a granodiorite pluton (C. Carson, unpubl. data 2002), that cuts the sequence. Accordingly, this migmatized metasedimentary sequence is considered to represent an uppermost, clastic-rock-dominated component of the PAg (Skulski *et al.* 2003b).

Structure

The Committee Bay area has been affected by two events of penetrative deformation (D_1 and D_2), polymetamorphism, and localized D_3 shortening (folding ± shearing) (Sandeman *et al.* 2001b, Sanborn-Barrie *et al.* 2002, 2003). The D_1 event involved development of northward-trending, variably inclined, west-vergent folds and associated northward-striking axial planar L < S fabrics that affect the PAg and widespread *ca.* 2.6 Ga plutonic rocks, providing a maximum age of *ca.* 2.6 Ga for D_1. Although L_1/S_1 fabrics are generally moderately to strongly developed, they are only locally preserved owing to the penetrative nature of subsequent D_2 strain. Typically, D_1 structures are recognized in the hinge zones of major F_2 folds, where they are oriented at a high angle to the D_2 shortening plane. In the southwestern CBb, however, the 800 km^2 Laughland Lake tonalite pluton has shielded D_1 folds and fabrics to its southwest and northeast from the penetrative effects of D_2 strain. This general area is the focus of this study and is discussed in more detail below. High-grade rocks of the northern migmatite subdomain preserve gneissic layering (S_1), defined by alternating biotite-rich and quartzofeldspathic layers.

The dominant penetrative structural elements of the Committee Bay region are attributed to D_2 (Sandeman *et al.* 2001b, Sanborn-Barrie *et al.* 2002, 2003). These include NE-trending F_2 folds, a NE-striking transposition ($S_2 \pm S_1$) foliation, and shallowly (<35°) plunging stretching lineations ($L_2 \pm L_1$). S_2 ($\pm S_1$) planes are mainly SE-dipping (30–70°), consistent with NW-directed shortening during D_2, and typically show stronger extensional strain relative to flattening strain (L > S). L_2 stretching lineations and F_2 axes are generally colinear and show plunge reversals wherein broad 50- to 100-km-wide domains of mainly shallow NE-plunging structures alternate with narrower 20-km-wide domains of moderate to shallow SW-plunging structures. These variations are interpreted to reflect the geometry of F_1 folded strata on which subsequent D_2 strain was imposed. D_2 is constrained to be broadly synchronous with *ca.* 1.85 Ga metamorphism in the northern migmatite subdomain (Carson *et al.* 2004). A minimum age for S_2 is provided by crosscutting monzogranite dykes that have been dated at *ca.* 1.815 Ga in the northern migmatite subdomain (Sanborn-Barrie *et al.*, unpubl. data) and at *ca.* 1.82 Ga in the southwestern Walker Lake intrusive complex (Skulski *et al.* 2003b).

Reworking of D_2 structures is manifested by two discrete sets of structures within the CBb. Reorientation of D_2 structures during layer-parallel (~NE-directed) shortening is best developed in the northeast (56P), where conjugate kink- to chevron-style F_3 folds are well developed along an ~80-km strike-length of the PAg supracrustal belt (Sanborn-Barrie *et al.* 2003). Late-stage, NE-directed shortening is also manifest in upright, gentle northwest-striking F_3 crossfolds in the western part of the belt (Sandeman *et al.* 2001b). Reworking of D_2 structures also occurs within two east-striking fault zones: the dextral, oblique-slip Amer fault zone in the southwest part of the belt, and the centrally located dextral, strike-slip Walker Lake shear zone (Fig. 2; Johnstone 2002, Johnstone *et al.* 2002). The D_3 event is considered to be *ca.* 1.81–1.78 Ga in age, based on *in situ* dating constraints from the central and eastern parts of the Prince Albert Group subdomain (Berman *et al.* 2003).

Metamorphism

Early investigations of the CBb by Schau (1978, 1982) documented a general increase in metamorphic grade from greenschist facies in the southwest, in the vicinity of the Laughland Lake tonalite (Fig. 2), through

FIG. 1. Regional geology of the western Churchill Province and environs. Abbreviations: Ag: Amer group, Amer fz: Amer fault zone, ATH: Athabasca formation, BLG: Baker Lake group, CBb: Committee Bay belt, CB: Cumberland batholith, CH: Central Hearne subdomain, GB: Great Bear arc, MRg: Mary River Group, Narsajuaq arc (NA), NWH: northwest Hearne subdomain, Pg: Piling Group, STZ: Snowbird tectonic zone, TH: Thelon formation, WB: Wathaman batholith, Wg: Woodburn group. Blue boxes show the location of the Committee Bay belt (Fig. 2). Locations referred to in text, mostly with reported *ca.* 2.4–2.3 Ga ages (violet squares and polygons), include: Angikuni Lake (Al), Boothia Peninsula (B), Beaverlodge area (Bl), East-Athabasca mylonite zone (E), Kramanituar complex (K), a region south of the MacDonald fault (M), southern (QM) and northern (Q) Queen Maud block, southern (Ts) and northern (Tn) Taltson basement complex, Thelon tectonic zone (Th), Western granulite domain (W), and two *ca.* 2.32 Ga samples from the Buffalo Head terrane. Note that *ca.* 1.87–1.85 Ga and 1.85–1.81 Ga granitic rocks are unsubdivided east of Hudson Bay. Hudson "protocontinent" (Roksandic *et al.* 1987) is outlined in Hudson Bay. Numbered faults (#1 and #2) show approximate positions of early (*ca.* 1.88–1.86 Ga) Trans-Hudson, northern sutures discussed in text.

upper amphibolite facies in the northwest and northeast. Available geochronology at that time was interpreted to indicate a Neoarchean age for the dominant metamorphism, with a low-grade Paleoproterozoic overprint. Figure 2 illustrates the general disposition of metamorphic zones, based largely on a petrographic evaluation of ~200 thin sections and field observations made during 1:100,000 scale mapping of the CBb (Sandeman *et al.* 2001a, b, Sanborn-Barrie *et al.* 2002, 2003, Skulski *et al.* 2002a, 2003a, b), with consideration of the work of Schau (1978, 1982) and Sandeman *et al.* (2001b), as well as reconnaissance-scale mapping and petrography by Thompson (1998). The lowest metamorphic grade is recognized in upper-greenschist-facies Chl–Cld–Ms and Chl–Ky–Ms (abbreviations after Kretz 1983) metapelitic rocks (Schau 1982) southwest of the Laughland Lake tonalite (Fig. 2). A relatively steep metamorphic gradient to the west and north, and a more gentle gradient to the east passes through lower-amphibolite-facies St–Grt–Bt±Crd–Ms and And–Bt–Ms±Crd metapsammite and metapelite, reaching the mid-amphibolite facies (Grt–Sil–Bt±Ms metapelite) within large portions of the central PAg subdomain, and the upper-amphibolite facies (Kfs–Sil–Grt±Crd metapelite) in the northern migmatite domain (Fig. 2). A low-pressure facies-series metamorphism is indicated by the widespread occurrence of andalusite in lower-amphibolite-facies metaquartzite and metapelitic rocks, and Grt–Crd–Kfs at the highest metamorphic grades, reached locally in the northern migmatite domain around locality 5 (Fig. 2; Carson *et al.* 2004).

The simple distribution of metamorphic zones depicted in Figure 2 belies a more complex metamorphic history, recently revealed by an *in situ* geochronological study in the northern migmatite subdomain (locality 5, Fig. 2; Carson *et al.* 2004). There, migmatitic rocks are interpreted to have formed through the superposition of similar-grade (mid- to upper-amphibolite facies) metamorphic events at *ca.* 2.35, 1.85, and 1.78 Ga (Carson *et al.* 2004). These authors demonstrated that the major deformation event (D_2) occurred at *ca.* 1.85–1.82 Ga, but textural ambiguities in the samples they studied obscured the significance of the *ca.* 2.35 and 1.78 Ga events. In this paper, we provide further insights into the tectonometamorphic evolution of the CBb gained from detailed mapping of the southwestern PAg subdomain, west of the Laughland Lake tonalite (Fig. 2), together with new constraints provided by samples that were collected for linked structural, metamorphic, and geochronological analysis.

Petrological Methods

Thermobarometry

Compositions of selected mineral for pressure (*P*) – temperature (*T*) estimates were determined using a Cameca SX–50 electron microprobe located at Geological Survey of Canada (Ottawa), employing four spectrometers, a range of natural and synthetic standards, and matrix corrections after Pouchou & Pichoir (1985). Analytical conditions for all phases were 20 kV accelerating voltage, with a 10 nA beam current. A 10 μm beam spot was used for feldspars, and a more focused beam (~3 μm) for garnet, biotite, staurolite, and cordierite.

Pressure–temperature estimates were calculated using the TWEEQU software (Berman 1991), which incorporates revised thermodynamic data for garnet, cordierite, and biotite (Berman & Aranovich 1996; TWQ version 2.02b; http://www.gis.nrcan.gc.ca/twq.html). The following independent set of equilibria were used for *P–T* calculations:

annite + pyrope = phlogopite + almandine (1)

3 anorthite = grossular + 2 sillimanite + quartz (2)

3 siderophyllite + 6 quartz + 2 grossular + almandine = 3 annite + 6 anorthite (3)

Equilibrium (3) is an important barometer for sillimanite- and muscovite-absent assemblages (Hoisch 1990), which are common in the K-poor metapsammite of the Prince Albert Group. For sillimanite-absent assemblages, equilibrium (2) yields a constraint on maximum pressure. For the samples of this study, ~0.3–0.5 kbar higher pressures were generally retrieved with equilibrium (2) than equilibrium (3), consistent with the high activity of sillimanite (0.9–0.95) estimated *via* forward modelling described below. For two samples in which calculated pressures were higher with equilibrium (3) than equilibrium (2), the latter values were adopted. Absolute errors of thermobarometric data are considered to be approximately ±50°C and 1 kbar (Essene 1989, Berman 1991), with appreciably smaller errors associated with relative differences between samples.

Phase diagram calculations

In order to help constrain *P–T*–t paths during multiple metamorphic events, the program DOMINO (De Capitani 1994; http://titan.minpet.unibas.ch/minpet/groups/theriak/theruser.html, August, 2003 version) was used to calculate phase diagrams in the system MnO–CaO–Na_2O–K_2O–FeO–MgO–Al_2O_3–SiO_2–H_2O. The components MnO, CaO, and Na_2O were included in addition to the KFMASH system in order to account for the important effects of Mn and Ca on the stability of garnet (*e.g.*, Spear 1993, Tinkham *et al.* 2003). Bulk compositions were determined by X-ray-fluorescence analyses of powdered rock samples. We consider the following phases in the construction of the phase diagrams: garnet, biotite, cordierite, sillimanite, andalusite, K-feldspar, plagioclase, staurolite, chlorite, chloritoid, white mica, quartz, and H_2O. All calculations used the thermodynamic dataset of Holland & Powell (1998), which includes Mn end-members. Activity–composition models employed in this study are given by Tinkham *et al.* (2003), with the biotite and chlorite models reparameterized for use with DOMINO (C. De Capitani, pers. communication). Some degree of mismatch with *P–T* results can be expected because the phase diagram and thermobarometric calculations utilize different thermodynamic datasets. However, we used TWEEQU thermobarometric results because its calibration of equilibrium (3) is based on experimental data directly constraining the properties of siderophyllite (Berman *et al.* 1995, Berman & Aranovich, in prep.).

An important variable influencing computed phase diagrams is the H_2O content of the bulk composition. It is generally agreed that saturation in H_2O (hydrous fluid present) results from the release of H_2O through prograde breakdown of hydrous minerals during low- to medium-grade metamorphism (*e.g.*, Spear 1993, Guiraud *et al.* 2001). However, the common preservation of minimally retrograded peak-metamorphic assemblages is good evidence that once liberated, H_2O migration prevents retrograde rehydration (Spear 1993, Giraud *et al.* 2001, Brown 2002). Thus, for polymetamorphic rocks, it is likely that fluid undersaturation may characterize all but the first metamorphism, particularly at temperatures lower than achieved during prior metamorphic events. Nevertheless, we have assumed H_2O saturation for all calculations, because the differences between fluid-absent and fluid-present phase relations at low temperatures do not affect our interpretations of the *P–T*–t paths followed by the rocks studied in this paper, whereas we avoid the complexity introduced through the dependence of the calculated stable assemblage on the assumed degree of H_2O undersaturation (Guiraud *et al.* 2001).

STRUCTURE AND PETROLOGY OF THE SOUTHWESTERN COMMITTEE BAY BELT

Structure

Preservation of early D_1 folds and fabrics in the strain shadows of the Laughland Lake tonalite pluton (Sandeman *et al.* 2001a, b), located in the southwestern part of the area (Fig. 2), highlight the importance of this part of the Committee Bay belt as a region with the potential to preserve *P–T*–t constraints on early regional tectonometamorphism. Both northeast and southwest of the Laughland Lake tonalite, a NNW- to NNE-striking S_1 foliation is defined at the outcrop scale, primarily by elongate porphyroblasts of garnet and amphibole in metavolcanic rocks, and andalusite and muscovite in metaquartzite, and andalusite, staurolite, and muscovite in metapelitic rocks. This S_1 fabric is generally parallel to bedding and is axial-planar to inclined, W-vergent F_1 folds (MacHattie 2002) that are recognized regionally across the Committee Bay belt (Sanborn-Barrie *et al.* 2002, 2003). In some mafic volcanic rocks, early hydrothermal alteration appears to have resulted in bedding-parallel zones of alteration enriched in Al or Ca (or both) which, after D_1 tectonometamorphism, are represented by bedding-parallel aluminosilicate-rich (*e.g.*, Figs. 3a, b) and diopside-bearing gneissic layering, respectively. In contrast to the strain-shadow regions of the synvolcanic pluton, where a single or prominent S_1 foliation can be recognized, a penetrative S_2 fabric is typically developed in rocks to its northwest and southeast. These relationships, and the weak foliation developed within the pluton, indicate that the pluton acted as a relatively competent body that shielded wallrocks in its proximity from the penetrative effects of D_2 strain that typify the northeastern CBb. Here, we provide constraints on the conditions and timing of development of the early tectonometamorphic fabric, and its subsequent reworking, from several localities west-southwest of the Laughland Lake tonalite (Fig. 2).

Typically throughout the southwestern strain-shadow, an early tectonometamorphic foliation (S_1) is recognized as a moderately developed, relatively straight, northward-striking, east-dipping foliation with little macroscopic indication of superimposed D_2 strain (Fig. 3a). This north-striking S_1 fabric is also locally intensely developed, and defines a straight, high-strain zone with a moderate to shallow easterly dip and very strong down-dip extensional lineation (Fig. 3b). Facing directions and the distribution of stratigraphic units suggest that this D_1 shear zone may have involved west-vergent thrusting, placing middle members of the Prince Albert Group structurally above upper wacke–metatexite exposed to the west. More typically, shallow to moderate east-dipping S_1 fabrics trend northeasterly, are locally folded, and exhibit variable development of an overprinting (S_2) foliation axial planar to these folds. In these regions, reorientation of S_1 during D_2 is apparent. For instance, at locality 1 (Fig. 2), $S_1 = S_0$ in muscovite – andalusite – staurolite metaquartzite is defined by ribbons of andalusite, muscovite and quartz, and is locally crenulated owing to overprinting D_2 strain (Fig. 3c). At locality 2 (Fig. 2), S_1 in altered mafic volcanic rocks is defined by highly elongate grains of garnet (6:1 aspect ratio) and aligned porphyroblasts of amphibole, that are variably folded and reoriented by D_2 (Fig. 3d). At these localities, and elsewhere in this region, S_1 fabrics are defined by porphyroblasts indicating metamorphism of these rocks prior to, or during, D_1 strain. Because garnet is not susceptible to the degree of plastic deformation required to generate a 6:1 aspect ratio, owing to the small number of slip systems available to activate, the preferred shape of garnet porphyroblasts defining S_1 at locality 2 support syntectonic (D_1) metamorphism (garnet growth) at amphibolite-facies (garnet–amphibole) conditions.

Beyond the southwestern strain-shadow of the Laughland Lake tonalite, rocks of the southwestern Committee Bay belt typically display a dominant north-

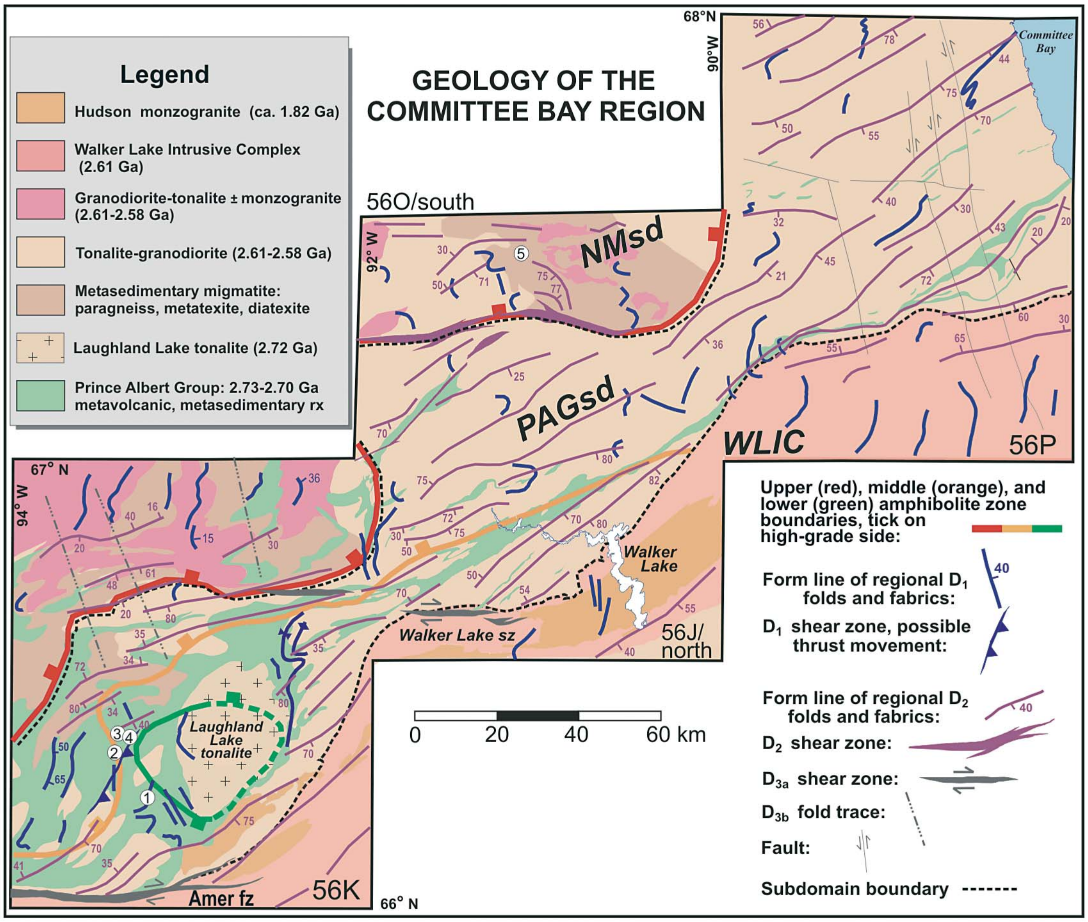

FIG. 2. Simplified geology [adapted from Sandeman *et al.* (2002, 2004), Skulski *et al.* (2003a, b)], structure, and metamorphic zones of the Committee Bay belt. Note sample localities 1–4 (this study) in the southwest Prince Albert Group subdomain (PAGsd) and locality 5 (Carson *et al.* 2004) in the northern migmatite subdomain (NMsd). WLIC: Walker Lake intrusive complex.

east-striking L–S fabric (S_2) that overprints a less prominent, variably reworked early foliation (S_1). In some cases, the early fabric is at a high angle to the overprinting S_2 fabric, such that the northerly trend of S_1 is consistent with D_1 structural trends in the strain-shadow regions. Commonly, however, the obliquity between the early fabric and the overprinting northeast-striking (S_2) fabric is moderate to small (<40°), suggesting variable rotation or transposition of S_1 during penetrative D_2 strain. The S_2 foliation in the southwestern CBb is defined by aligned biotite and preferred shape-orientation in quartz, with little preferred shape-fabric defined by garnet or staurolite porphyroblasts.

Metamorphism

Because of the paucity of low-variance pelitic rocks within the southwestern strain-shadow, much of our insight into the polyphase metamorphic history of the southwestern CBb has been obtained from a corridor ~4 km wide west of the Laughland Lake tonalite in an area previously recognized to have a complex polymetamorphic history (Sandeman *et al.* 2001b). This region is dominated by lower-amphibolite-facies, K-poor (muscovite-absent), metapsammitic rocks interlayered with more aluminous, pelitic horizons (localities 3 and 4; Fig. 2). In this area, S_1 fabrics are preserved, but are

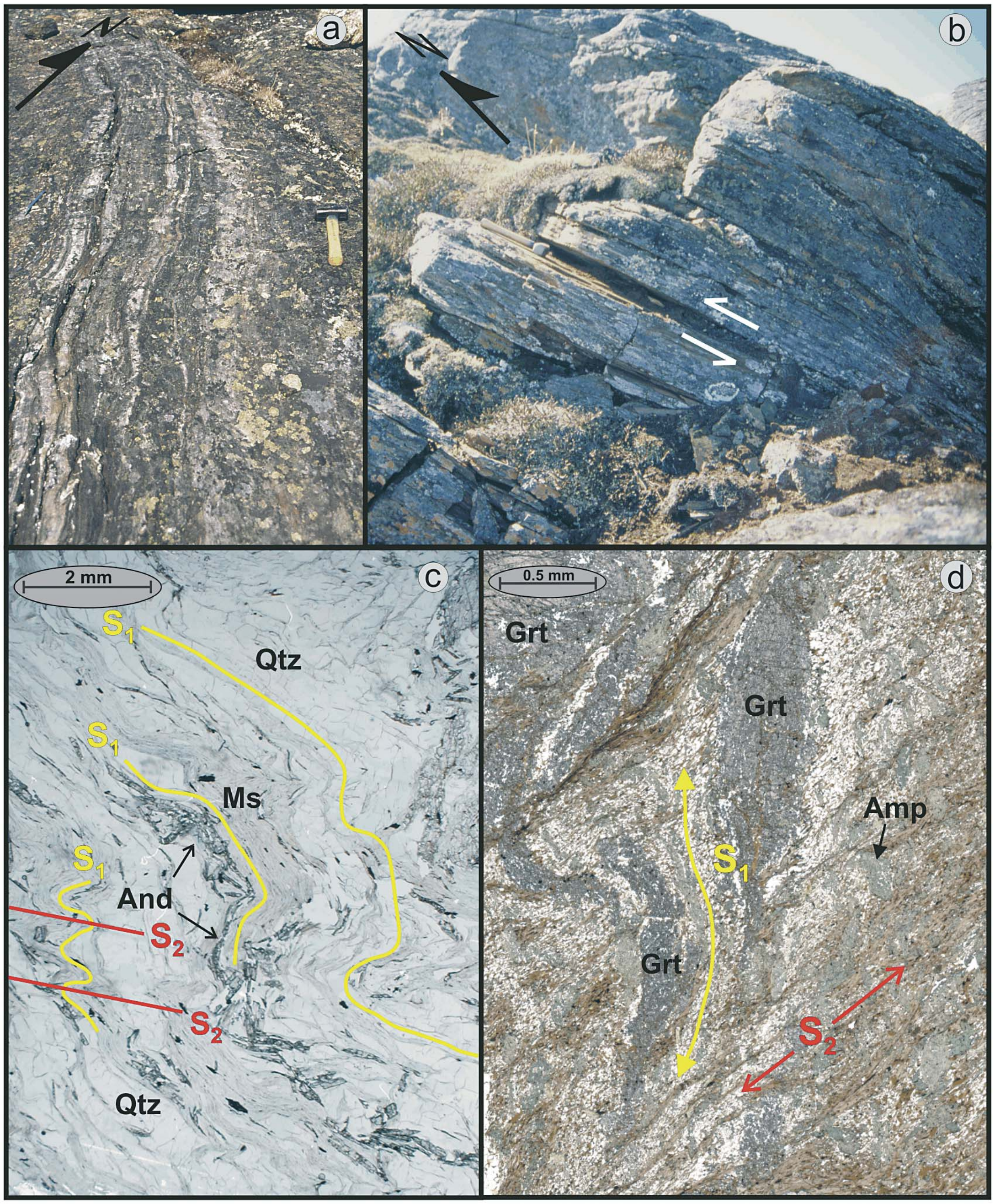

FIG. 3. (a) Gneissic $S_1 = S_0$ fabric oriented 325/50° in altered mafic metavolcanic rocks from locality 2 (Fig. 2); 26-cm-long hammer for scale. (b) D_1 shear zone oriented 017/22° with potential west-vergent thrust displacement, located ~1 km southeast of locality 2; 26-cm-long hammer for scale. (c) Photomicrograph of metaquartzite (plane-polarized light) from locality 1 (Fig. 2) with $S_1 = S_0$ oriented 135/80°, defined by andalusite, muscovite, and elongate quartz, and local crenulation of S_1 by northeast-trending F_2 microfolds. (d) Photomicrograph of altered mafic metavolcanic rock (plane-polarized light) shown in (a) with elongate garnet and shape-preferred orientation of amphibole and plagioclase defining S_1 at 325/50°, crenulated and overprinted by spaced S_2 cleavage at 040/78°, defined primarily by biotite. Mineral abbreviations from Kretz (1983); Amp: amphibole.

penetratively reoriented by D_2 strain such that exposures are dominated by a composite northeast-striking (045–070°) foliation, and thin sections oriented parallel to the northeasterly trending L_2 display a composite fabric in which S_1 and S_2 are indistinguishable. However, because S_2 dips more steeply to the southeast than S_1, thin sections oriented perpendicular to L_2 generally display two oblique foliations (S_1 and S_2), so that parageneses of different age can be distinguished *via* the relationships of porphyroblasts to these fabrics. These relationships are described below for two staurolite- and garnet-bearing samples (z7641 and z7635), collected 120 m apart at locality 3 (Fig. 2), for which *in situ* geochronological and quantitative metamorphic data are also presented. Adjacent to these sample locations (locality 3_{And}; not shown on Fig. 2), as well as 3 km to the east (locality 4, Fig. 2), andalusite-bearing metapelitic rocks provide important qualitative constraints. For notational simplicity in this paper, we refer to syn- to post-S_1 (pre-D_2) parageneses as M_1, and texturally related, syn- to post-S_2 assemblages as M_2, with letters (a, b, c) indicating the relative timing of porphyroblast growth with respect to fabric development during each metamorphic event. Several metamorphic features presented below are also suggestive of a cryptic, pre-S_1 metamorphism that we refer to here as M_0.

Highly aluminous, metapelitic rocks at locality 3_{And} comprise up to 90% andalusite porphyroblasts in a matrix of muscovite, biotite, chlorite, plagioclase, quartz, and ilmenite. Muscovite, with less abundant biotite, define an early foliation (S_1) that is strongly reoriented adjacent to S_2 cleavage planes. Some blades of both micas also crosscut these fabric elements, together with late sprays of chlorite. Although obscured by the degree of D_2 deformation and the small proportion of matrix to porphyroblast at this locality, textural relationships suggest three generations of andalusite crystallization. The earliest generation is enveloped by S_2 and contains randomly oriented inclusions of embayed kyanite, sillimanite sheaves, euhedral staurolite, and muscovite (Fig. 4a). The random orientation of these inclusions (Fig. 4a) is indicative of low-strain crystallization which, given that these porphyroblasts are wrapped by S_2, took place during, or more likely prior to D_1. This paragenesis may represent the product of regional contact metamorphism (M_0), which is indicated to have occurred in the belt at *ca.* 2.58 Ga from low-(Th/U) zircon rims analyzed in *ca.* 2.6 Ga granitic rocks that intrude the CBb (Fig. 2; Skulski *et al.* 2003b). Low-strain, *ca.* 2.58 Ga (contact?) metamorphism is similarly suggested in the eastern CBb by *ca.* 2.58 Ga SHRIMP data on monazite inclusions in a garnet core that displays randomly oriented inclusions of quartz (Berman *et al.* 2003). Andalusite that deflects S_2 and contains mats of aligned fine-grained sillimanite is interpreted as a syn- to post-S_1 (M_1) porphyroblast. M_2 andalusite locally cuts S_2-parallel biotite at locality 3_{And}, and overgrows a strongly reworked S_1 fabric in lower-grade muscovite–chlorite phyllites at locality 4 (Fig. 4b). In summary (Table 1), aluminous metapelitic samples at localities 3_{And} and 4 provide textural evidence consis-

TABLE 1. TEXTURAL FEATURES FROM z7641 AND NEARBY ANDALUSITE-BEARING METAPELITES

Defm[1]	Metm[2]	Rdefm[3]	Porphyroblast	Character, relationship to tectonic fabrics
	M_0	pre-D_1	andalusite	overgrows randomly-oriented Sil sheaves, St, Chl, Ms, embayed Ky
D_1	M_{1a}	syn-D_1	staurolite	elongate, overgrows weak, fine-grained S_1
	M_{1a}	syn-D_1	plagioclase	elongate grains with quartz, ilmenite inclusions
	M_{1b}	late- to post-D_1	staurolite	equant, overgrows coarse S_1; unzoned
	M_{1b}	syn- to post-D_1	andalusite	contains mats of aligned Sil; deflects S_2
D_2 *P~5.9 kb*	M_{2a}	late-D_2	garnet core	deflects S_2
P~5.1 kb	M_{2b}	post-D_2	garnet rim	cuts S_2
	M_{2b}	post-D_2	staurolite	overgrows reworked S_1, cuts S_2
	M_{2b}	post-D_2	plagioclase	clear grains that cut S_2
	M_{2b}	post-D_2	andalusite	overgrows & cuts strong, straight S_2

[1]Deformation event; [2] Metamorphic chronology (relative crystallization sequence)
[3] Metamorphism-deformation relationship

tent with three episodes of andalusite growth: prior to D_1, post-D_1, and post-D_2.

Sample z7641 (*UTM 482429/7364291, zone 15; NAD 83*)

Sample z7641 is a staurolite-rich semipelitic sample containing the assemblage St–Bt–Grt–Pl–Qtz–Ilm–Py, with minor post-S_2 chlorite and muscovite. The sample is characterized texturally by mm- to cm-wide domains with a penetrative, generally shallowly dipping (0–40°) S_1 foliation preserved in, and adjacent to, staurolite porphyroblasts, and a steeply southeasterly dipping S_2 cleavage (~075/76°) that separates variably reoriented S_1 domains (Fig. 4c). The inferred sequence of growth of metamorphic minerals and fabric development is summarized for this locality (and adjacent andalusite-bearing metapelite, described above) in Table 1. Two generations of staurolite can be distinguished in thin sections oriented perpendicular to the NE-trending L_2. M_1 staurolite occurs in S_1 domains as mm-sized porphyroblasts that are wrapped by S_2 biotite and contain a straight internal fabric defined by quartz, ilmenite and, rarely, chlorite and biotite inclusions (Fig. 4c). This internal fabric is parallel to the weakly preserved, external S_1 fabric defined by aligned biotite in a matrix of elongate quartz and plagioclase (Figs. 4c, 5a, b). This staurolite is considered post-D_1 (M_{1b}), as it has overgrown, but is not enveloped by, the well-established S_1 foliation in this rock. Certain textural features also point to syn-D_1 growth. For instance, some staurolite porphyroblasts (M_{1a}) display a high aspect-ratio (between 3:1 and 5:1) indicative of D_1 strain-induced, preferred direction of growth (Fig. 5b). Elongate M_{1a} staurolite also invariably contains a significantly weaker internal fabric (Fig. 5b, Table 1), suggesting that these grains grew early in the S_1-forming event, prior to more equant and generally coarsely included grains (M_{1b}; Figs. 4c, 5a, b). The fact that some near-equant staurolite also contains a weak internal fabric likely relates to variations in original grain-size of the matrix or rates of growth of individual porphyroblasts.

M_1 staurolite is interpreted to predate D_2 strain because internal trails of inclusions are straight and apparently unaffected by D_2. Reworking of M_1 staurolite during D_2 is manifest by bent and broken, elongate porphyroblasts, and reorientation of staurolite-rich S_1 domains toward S_2. M_2 staurolite cuts biotite that defines S_2 and overgrows domains of reworked S_1 without deflecting S_2-parallel biotite (Fig. 5c, Table 1).

Garnet in sample z7641 forms sparse, late- to post-D_2 (M_2) porphyroblasts 0.1–1.5 mm across that generally cut (Figs. 4c, 5a; M_{2b} in Table 1), but in places slightly deflect S_2-parallel biotite (Fig. 5d; M_{2a} in Table 1). Two types of plagioclase are evident. M_1 plagioclase forms elongate, fractured grains that help define the S_1 fabric, and that are clouded with quartz and ilmenite inclusions. M_2 plagioclase occurs as a rim on M_1 plagioclase and as recrystallized grains that cut S_2-parallel biotite. In summary, growth of metamorphic minerals relative to fabric development in z7641 is recognized in two main stages (Table 1): M_1 involved syn-D_1 biotite and plagioclase, and syn- to post-D_1 staurolite. M_2 involved syn-D_2 biotite, late- to post-D_2 garnet, and post-D_2 staurolite and plagioclase.

Representative compositions of minerals for z7641 are presented in Table 2. Compositional profiles of garnet porphyroblasts show uniform Fe/(Fe + Mg) between 0.893 and 0.901 across broad calcic cores ($X_{Grs} = 0.062$) that are zoned to less calcic ($X_{Grs} = 0.043$) rims (Fig. 6). The M_1 plagioclase shows little variation in composition ($0.30 < X_{An} < 0.32$). M_2 plagioclase is slightly more sodic ($0.24 < X_{An} < 0.28$). No compositional differences were detected in the biotite that defines either S_1 or S_2. Given the late-D_2 nature of M_2 garnet and M_2 plagioclase, these phases are interpreted to have been in equilibrium. The large modal abundance of plagioclase relative to garnet is compatible with the hypothesis that garnet composition adapted to changing *P–T* conditions, whereas plagioclase composition remained essentially constant. Using equilibria (1) and (3), core compositions of the garnet together with M_2 plagioclase and biotite yield 570ºC and 5.9 kbar. Rim compositions of adjacent, but non-touching garnet, M_2 plagioclase, and biotite record *P–T* conditions of 585°C and 5.1 kbar, suggesting decompression of ~0.8 kbar at near-peak M_2 temperatures.

Phase-equilibrium relationships relevant to z7641 and aluminous metapelites at locality 3_{And} are summarized in a phase diagram calculated with the bulk chemical composition of z7641 (Fig. 7). The occurrence at the locality 3_{And} of embayed kyanite, together with euhedral staurolite and sillimanite inclusions in andalusite, is consistent with a near-isobaric or clockwise *P–T*–t path for M_0 (dashed *P–T*–t path in Fig. 7), passing near the aluminosilicate triple point on the prograde path, and into the stability field of andalusite near the thermal maximum and on the retrograde path. Peak M_0 temperatures are constrained by the occurrence of sillimanite and staurolite inclusions to have exceeded the aluminosilicate triple point and the first appearance of staurolite at 520ºC at ~4 kbar (on the basis of phase diagram phase-relations for an andalusite-rich sample), respectively. The absence of M_0 staurolite recognized in sample z7641 suggests that the maximum temperature did not greatly exceed the first appearance of staurolite, calculated at ~530°C and 4 kbar (Fig. 7).

Computed phase-relationships for z7641 indicate that garnet is stable above ~4.5 kbar at 540°C and above 560ºC at pressures as low as ~3 kbar. The absence of garnet from the staurolite-bearing M_1 assemblage thus constrains M_1 to *P–T* conditions lower than ~4.5 kbar and 560 °C, in accord with the M_1 *P–T*–t path defined by thermobarometric data for sample z7635 discussed below (square symbols in Fig. 7; Table 2). The calculated field of stability of the peak M_2 assemblage, St–

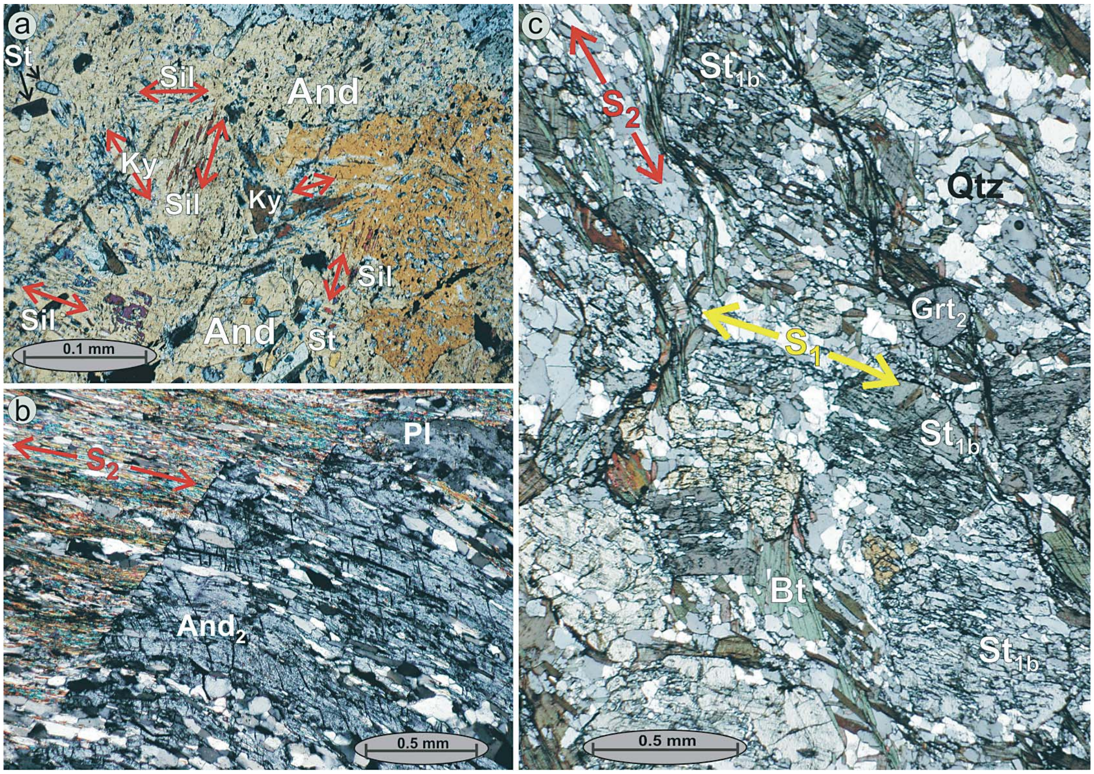

FIG. 4. Photomicrographs showing: (a) randomly oriented kyanite, sillimanite sheaves, and staurolite within M_0 andalusite at locality 3_{And}, with red arrows highlighting random orientation of inclusions. (b) Post-S_2 (M_2) andalusite (And_2) overgrowing strong S_2 fabric at locality 4. (c) Staurolite-rich domain of sample z7641 with shallowly SE-dipping S_1 fabric preserved within, and external (most evident in aligned biotite just above "S_1") to, late- to post-S_1 (M_{1b}) staurolite (St_{1b}) porphyroblasts. Note more steeply dipping, spaced, S_2 cleavage defined by partial re-alignment of biotite (Bt), overgrown by post-S_2 garnet (Grt_2).

Grt–Bt–Pl–Qtz–H_2O, occurs above terminal breakdown of chlorite at ~580°C, in good agreement with thermal peak conditions calculated with thermobarometry (circle symbols in Fig. 7). In addition to predicted and observed compositions of garnet being in excellent accord, computed compositional and modal isopleths offer strong support for the *P–T–*t path inferred from thermobarometric data and the occurrence of post-S_2 andalusite in adjacent metapelitic rocks at locality 3_{And}. Specifically, the moderate slope of X_{Grs} isopleths combined with the steep slope of Fe/(Fe + Mg) isopleths (shown only in the St–Grt–Bt–Pl–Qtz–H_2O field on Fig. 7) are compatible with the proposal that the observed zoning of the garnet [core to rim decrease in X_{Grs} at constant Fe/(Fe + Mg)] was produced during near-isothermal decompression. In addition, modal isopleths of garnet are subparallel to the steep Fe/(Fe + Mg) isopleths, consistent with garnet stability along the depicted path of M_2 decompression.

Sample z7635 (*UTM 482478/ 7364396, zone 15; NAD 83*)

Sample z7635 is a semipelitic schist that displays a penetrative, northeast-striking (~060º), moderately (<40º) east- or west-dipping S_1 fabric defined by aligned biotite within a quartz–plagioclase shape fabric that is parallel to compositional layering (S_0). This rock also carries a steep, southeasterly dipping, spaced (penetrative) S_2 cleavage (Fig. 8a) oriented approximately 070/65º. The sample contains the assemblage Grt–St–Bt–Pl–Qtz–Ilm–Py, with <5% retrograde, post-S_2 chlorite and muscovite. Various types of garnet and staurolite can be distinguished on the basis of textural and compositional variations. These are summarized in Table 3 relative to the established metamorphic (M_0–M_2) and deformation (D_1 and D_2) events, and described below.

All garnet porphyroblasts are enveloped by S_2. The earliest generation of garnet, designated M_0, forms

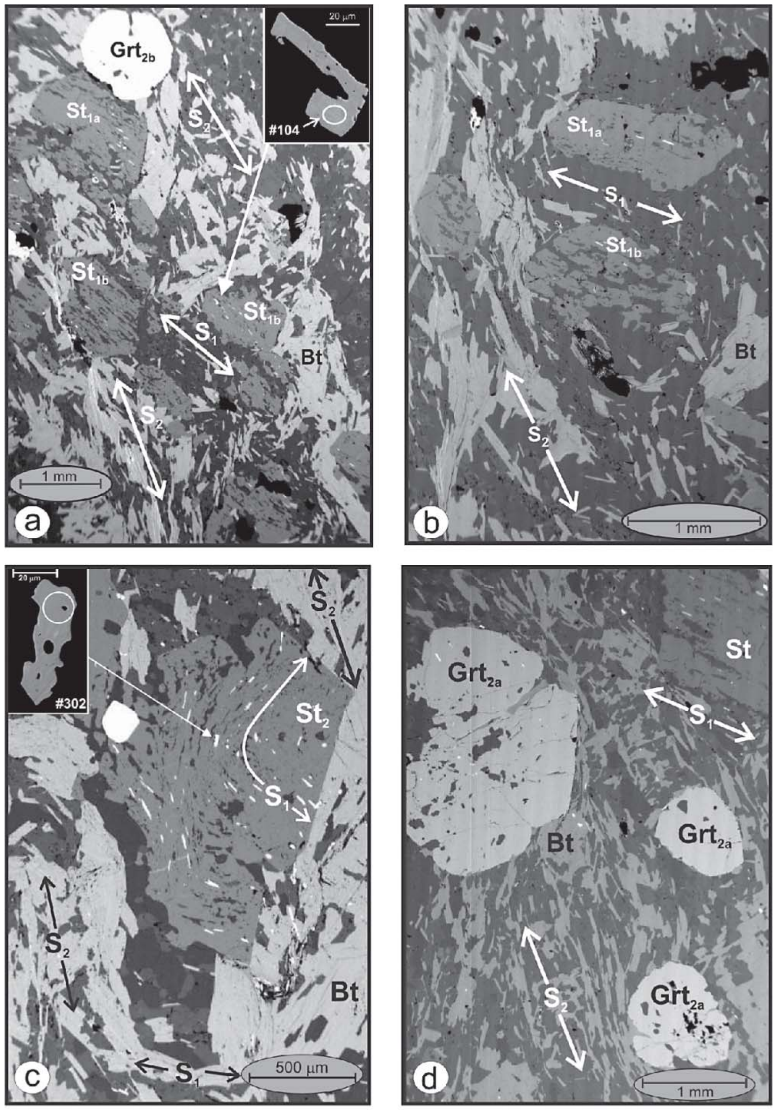

FIG. 5. Back-scattered-electron images of sample z7641 showing: (a) S_1 defined by, and preserved within, staurolite (St) porphyroblasts. Note variation among porphyroblasts in degree of development of internal inclusion-trail (ilmenite–quartz) fabric (S_1). Post-S_2 garnet overgrows steeply dipping S_2 foliation defined mainly by biotite (Bt); inset shows SHRIMP analysis-spot on monazite inclusion. (b) Staurolite porphyroblasts preserving internal S_1 oblique to external S_2 (~050/75°). Note the textural evidence for syntectonic growth of staurolite provided by elongate (syn-S_1) staurolite with weak internal fabric (M_{1a}) adjacent to more equant (late- to post-S_1) staurolite with well-developed, coarse-grained internal fabric (M_{1b}). (c) Late- to post-S_2 staurolite (M_2) that has overgrown a reworked (folded) S_1 fabric partly defined by elongate monazite (inset). (d) Late- to post-S_2 garnet porphyroblasts.

subhedral porphyroblasts 5–15 mm across that are inclusion-poor, but may contain scattered domains with a faint, fine-grained quartz or quartz–ilmenite inclusion fabric (Fig. 8b) that is steeply NW-dipping and discordant to all other external and internal tectonic fabrics. In contrast, M_1 garnet contains a ~NW-striking, shallowly dipping internal fabric that is parallel to the external S_1 fabric and discordant to the external S_2 (Figs. 8c–f). The M_{1a} garnet forms elongate, 1×4–7 mm grains (upper garnet in Figs. 8c and 9b with higher Mn content in the core region, indicating earlier crystallization relative to the lower garnet in these figures; see below). The M_{1b} garnet occurs as equant, euhedral to partly embayed crystals 5–20 mm wide, generally with an inclusion-free rim (Fig. 8d). The M_{1c} garnet occurs as smaller, roughly equant poikiloblasts up to 7 mm in diameter (lower garnet in Fig. 8c). The grain size of quartz, ilmenite and, rarely, chlorite that define the internal fabric of M_1 garnet displays a fairly consistent increase from M_{1a} (Fig. 8c, upper), M_{1b} (Fig. 8d) through M_{1c} (Figs. 8c (lower garnet), 8e) garnet, sug-

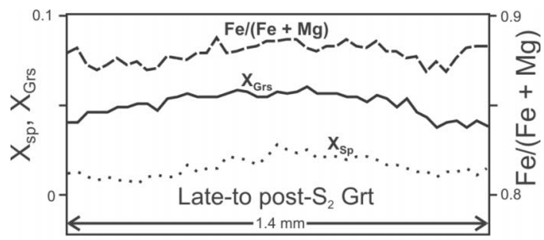

FIG. 6. Compositional profile of garnet porphyroblast in sample z7641.

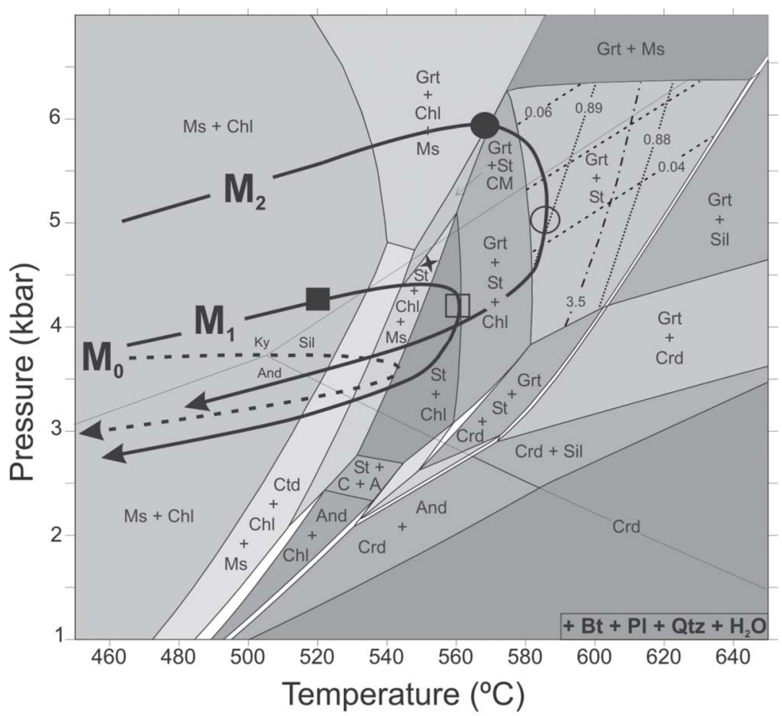

FIG. 7. Phase diagram calculated with the DOMINO software (De Capitani 1994) for sample z7641 (bulk composition in mole %: 66.94 SiO_2, 13.10 Al_2O_3, 9.46 FeO, 4.55 MgO, 1.74 CaO, 1.94 K_2O, 2.23 Na_2O, 0.03 MnO). All stability fields include Bt + Pl + Qtz + H_2O. Some stability fields less than five degrees in width have been omitted or not labeled for clarity. Shading of stability fields is independent of the variance, which ranges from 3 to 5. Star symbol shows aluminosilicate triple point estimated by Pattison (1992). In the St–Grt–Bt–Pl–Qtz–H_2O field, dotted, dashed, and dash–dot lines show isopleths of Fe/(Fe + Mg), X_{Grs}, and garnet modal percentage, respectively. *P–T*–t paths based on petrographic interpretations (M_0) and *P–T* results: circles show maximum-*P* (filled) and maximum-*T* (unfilled) M_2 conditions based on z7641 results; square symbols indicate prograde (filled) and peak (unfilled) M_1 conditions derived for z7635.

gesting M_1 garnet growth during the progressive development of S_1. Although these differences in the grain size of inclusions could be attributed to primary variations, the M_{1a} garnet (Fig. 8c, upper) displays a ~3.5:1 aspect-ratio that is consistent with strain-induced preferred growth during D_1, whereas the more equant habit (aspect ratio <1.5:1) of M_{1b} and M_{1c} garnet suggest late- to post-D_1 growth. In addition, chemical differences summarized below support a general progression from M_{1a} through M_{1c} growth. The M_2 garnet forms a sporadic partial rim ~50 – 120 μm wide on earlier garnet in proximity to matrix plagioclase (Fig. 8f). The width of

TABLE 2. REPRESENTATIVE MINERAL COMPOSITIONS AND THERMOBAROMETRIC RESULTS

Sample	z7641				z7635											
Mineral[1]	Grt-2a	Grt-2b	Bt	Pl	Grt-2	Bt	Pl	Grt-2	Bt	Pl	Grt-1c	Bt	Pl	Grt-1b	Bt	Pl
Spot[2]	core	rim	m	m	ir	m	m	ir	m	m	c	inc	inc	mid	inc	inc
Anal#[3]	D-19	D-41	D-3	D-26	D2-2	D2-4	D2-2	B3-89	B3-2	B3-7	C-128	C-35	C-45	D1-71	D1-6	D1-6
SiO_2	36.5	36.4	34.1	61.8	36.9	34.4	59.9	36.6	34.2	58.6	36.7	33.9	60.0	36.8	35.1	61.0
TiO2	0.1	0.0	1.6	—	0.0	1.7	—	0.1	1.5	—	0.0	1.6	—	0.1	1.4	—
Al_2O_3	21.1	21.0	19.4	23.8	21.2	19.5	25.4	21.0	19.6	26.2	20.9	19.7	25.4	20.8	18.8	24.6
FeO	37.3	37.1	21.8	0.2	36.8	20.0	0.2	36.2	20.5	0.2	37.2	19.3	0.1	37.2	18.6	0.1
MgO	2.3	2.6	8.8	—	2.5	9.2	—	2.3	8.8	—	2.8	9.5	—	2.6	9.9	—
CaO	2.2	1.5	—	5.1	2.8	—	6.6	3.5	—	7.8	1.8	—	7.0	1.8	—	6.3
MnO	1.0	0.6	0.1	—	0.4	0.1	—	0.7	0.1	—	0.2	0.1	—	0.4	0.0	—
Na_2O	—	—	0.3	8.8	—	0.3	7.8	—	0.3	7.2	—	0.1	7.4	—	0.3	8.2
K_2O	—	—	7.9	0.0	—	8.6	0.1	—	8.9	0.0	—	8.7	0.1	—	8.9	0.0
F	—	—	0.2	—	—	0.0	—	—	0.1	—	—	0.1	—	—	0.5	—
	100.6	99.3	94.4	99.7	100.7	94.1	100.0	100.3	94.5	100.0	99.8	94.0	100.0	99.6	93.2	100.2
Fe/(Fe+Mg)	.90	.89	.58		.89	.55		.90	.57		.88	.53		.89	.51	
X_{Ca}	.062	.043		.243	.079		.317	.099		.374	.052		.341	.049		.298
P[4]	5.9		5.1			6.1			6.5			4.3			4.6	
Pmax[5]	<6.4		<5.4			<6.4			<6.8			<4.2			<4.3	
T°C[6]	570		585			575			580			560			520	
Interp[7]	M_2 max-P		M_2 late			M_2 max P			M_2 max P			M_1 peak T			M_1 prograde	

[1] Grt-# = Metamorphism-# garnet
[2] Spot location: c = core, r = rim, ir = inner rim, mid = midway between core and rim, m = matrix, inc = inclusion
[3] Thin section - analysis number
[4] P(kbar) determined with equillibrium #3
[5] maximum P(kbar) determined with equillibrium #2
[6] T(°C) determined with equillibrium #1
[7] Interpretation of P-T result

TABLE 3. SUMMARY OF TEXTURAL FEATURES FROM z7635

Defm[1]	Metm[2]	Rdefm[3]	Porphyroblast	Character, relationship to tectonic fabrics	MnO[4]
	M_0	pre-D_1	garnet	5-15 mm; inclusion-poor; may contain weak internal fabric at high angle to S_1; growth zoned	3-6
	M_0	pre-D_1	staurolite	10-15 mm; no internal fabric	
D_1	M_{1a}	syn- to post-D_1	staurolite	10-12 mm; variably developed internal fabric parallel to S_1	
	M_{1a}	syn-D_1	garnet	elongate, overgrows fine-grained S_1; growth zoned	3-5
P~4.3 kb	M_{1b}	late- to post-D_1	garnet	equant, overgrows moderate S_1; growth zoned	1-5
P~4.2 kb	M_{1c}	late- to post-D_1	garnet	equant, overgrows coarse S_1; unzoned	<1
D_2 P~6.3 kb	M_2	pre- to post-D_2	garnet	high Ca rims, unclear relationship to S_2	0.7
	M_{2b}	late- to post-D_2	staurolite	< 1 mm; randomly oriented; aligned with, and overgrowing S_2	

[1]Deformation event; [2] Metamorphic chronology (relative crystallization sequence)
[3] Metamorphism-deformation relationship; [4]core MnO (wgt. %)

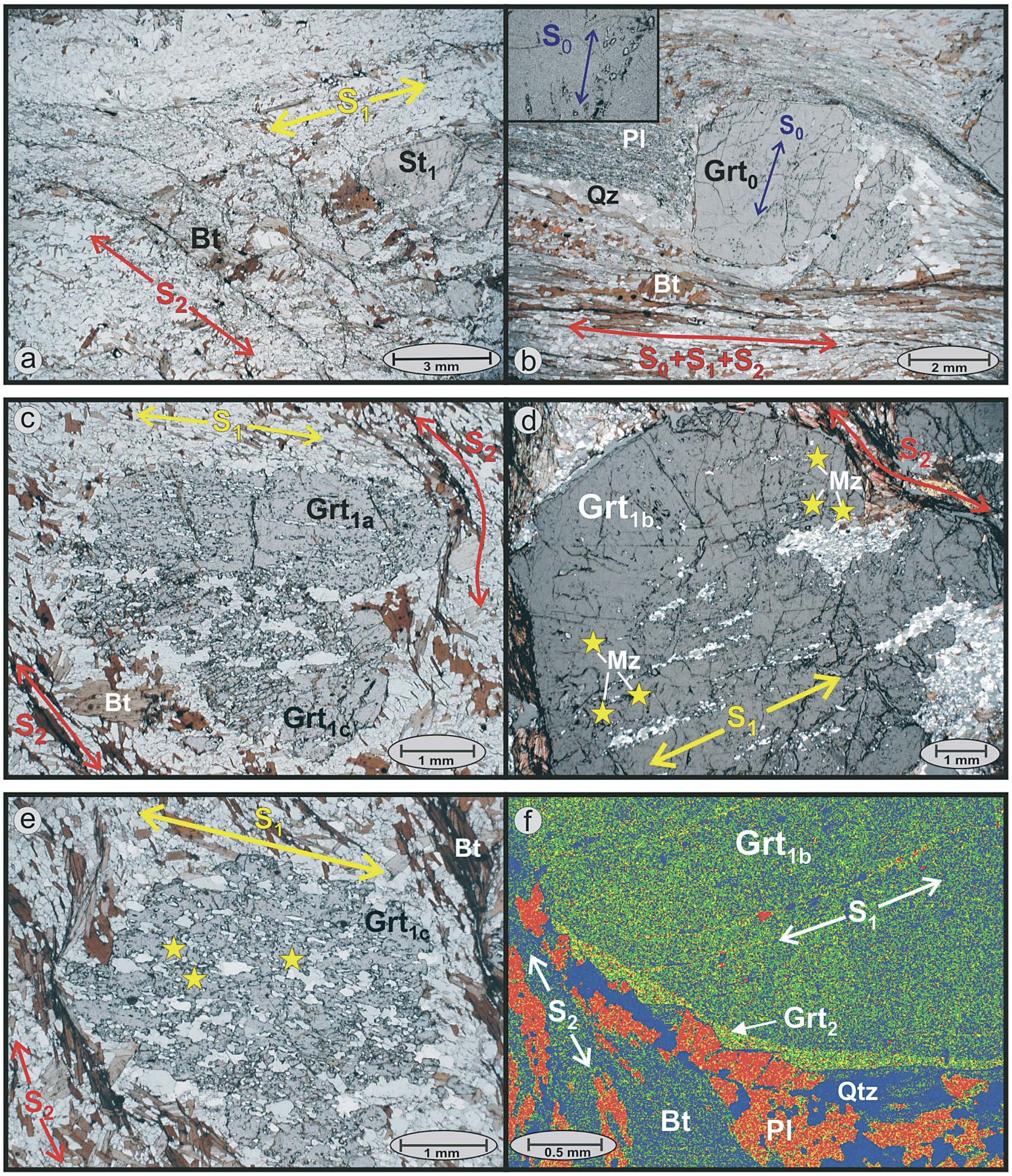

FIG. 8. Photomicrographs of z7635 showing: (a) shallowly dipping S_1 defined by biotite (Bt) and quartz–plagioclase elongation, transected by southeast-dipping S_2 cleavage. Note M_1 staurolite with coarse internal fabric parallel to S_1. Section perpendicular to L_2. (b) M_0 garnet enveloped by composite S_0 + S_1 + S_2 fabric containing steep, faint SW-dipping internal fabric (S_0). Section parallel to L_2. (c) Elongate, weakly included M_{1a} garnet (upper) and more equant, coarsely included M_{1c} garnet (lower), both enveloped by S_2 foliation. Section perpendicular to L_2. (d) M_{1b} garnet with monazite inclusions (yellow stars) restricted to the outer 1 mm of the garnet rim. Section perpendicular to L_2. (e) M_{1c} garnet wrapped by S_2 foliation. Note occurrence of monazite inclusions (yellow stars) throughout core and rim. Section perpendicular to L_2. (f) Ca X-ray map of high-Ca, M_2 garnet rim on M_{1b} garnet. Section perpendicular to L_2.

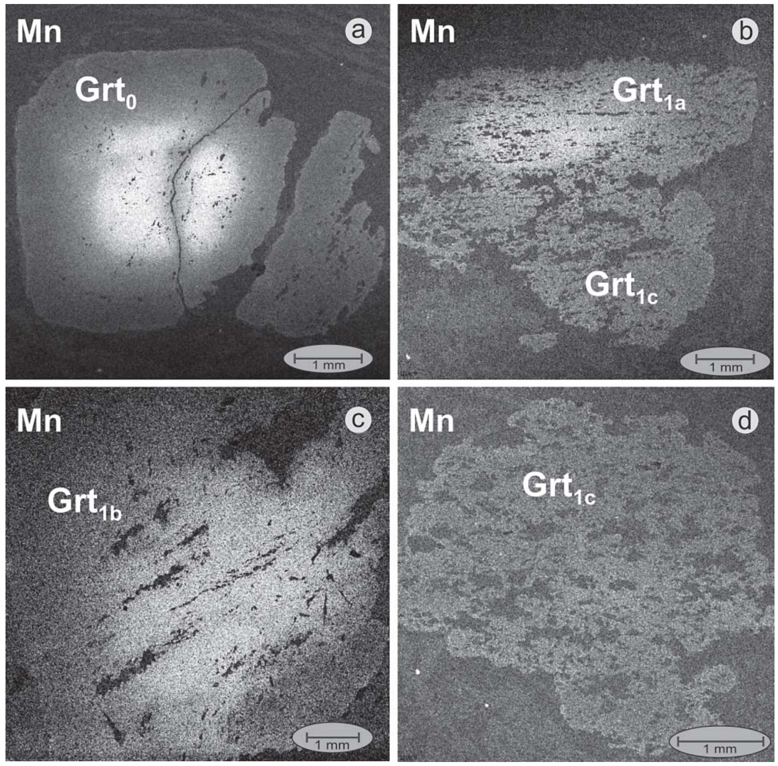

FIG. 9. Mn X-ray maps of different types of garnet in z7635 (brighter regions have higher Mn concentrations). (a) M_0 garnet with well-defined growth zoning. (b) Composite M_{1a} (upper zoned) and M_{1c} garnet (lower unzoned). (c) M_{1b} garnet with less pronounced growth-zoning. (d) Unzoned M_{1c} garnet.

such rims is not sufficient to indicate whether M_2 garnet grew pre-, syn-, or post-S_2 fabric formation. Enhancement of the width of M_2 garnet adjacent to microfractures suggests formation of some of the M_2 garnet *via* diffusional re-equilibration, whereas rims up to 120 μm wide with no visible fractures suggest growth of M_2 garnet (Fig. 8f).

Distinct compositional differences characterize some of the garnet types (Fig. 9, 10; Tables 2, 3). The M_0 garnet porphyroblasts (Figs. 9a, 10a) exhibit well-defined growth-induced zoning, with Mn, Ca, and Fe/(Fe + Mg) decreasing from core [~3–6 wt% MnO, ~3 wt% CaO, Fe/(Fe + Mg) = 0.93] to rim [<0.5 wt% MnO, 1.7–1.8 wt% CaO, Fe/(Fe + Mg) 0.88 or 0.89]. Crystals of M_{1a} and M_{1b} garnet also are growth-zoned, with M_{1a} core compositions (Figs. 9b, 10b) similar to, but generally slightly lower in Mn (~3–5 wt% MnO) and Ca (~2.2–2.4 wt% CaO) than M_0 cores. The M_{1b} garnet cores display more variable concentrations of Mn, ranging between 1 and 5 wt% (Figs. 9c, 10c; Table 1). The M_{1c} garnet is unzoned (Figs. 9d, lower part of 10b, 10d), with low Mn, Ca, and Fe/(Fe + Mg) equivalent to M_0 and M_1 garnet rims. An age progression from M_{1a} to M_{1c} garnet is suggested by the strong decrease in concentration of Mn in the core, which can be considered as a proxy for crystallization sequence (*e.g.*, Spear & Daniel 2003). M_2 garnet (Figs. 8f, 10a, 10d) is markedly higher in Ca (2.8–3.8 wt% CaO) than host garnet rims with <2 wt% CaO.

Three textural varieties of staurolite also occur in z7635 (Table 3). Several large (10–15 mm) porphyroblasts of staurolite that lack an internal fabric may have grown during M_0. The M_1 staurolite forms 8–12 mm porphyroblasts (Fig. 8a) with a variably developed internal fabric that is parallel both to the external S_1 fabric and to the inclusion fabric in M_1 garnet, consistent with M_1 staurolite and garnet growth during the same metamorphic event. The M_2 staurolite occurs as small (<1 mm), subhedral to euhedral laths that are generally randomly oriented, but locally are aligned parallel to the S_2 cleavage. The textural and chemical observations described above and summarized in Table 3 are interpreted to indicate three main generations of porphyroblast growth in z7635: M_0 involved pre-D_1 garnet and staurolite, M_1 involved syn-to post-D_1 garnet (M_{1a}, M_{1b}, M_{1c}) and staurolite, and M_2 involved late- to post-D_2 staurolite and garnet with an unclear relationship to D_2.

P–T estimates for different types of garnet are listed in Table 2 and shown in Figure 11. Prograde M_2 conditions averaging ~580°C and 6.3 kbar (solid diamond symbol in Fig. 11) are based on core compositions of M_2 garnet, together with nearby, but non-touching matrix plagioclase and biotite, which show no significant compositional variation with textural setting. These *P–T* conditions accord well with those recorded by M_2 garnet in z7641 (570°C and 5.9 kbar; circle symbols in Fig. 11). Near-peak M_1 conditions (~560°C and 4.2 kbar; open square symbol in Fig. 11) were derived both from the compositions of (*i*) a M_{1c} garnet core, a biotite lath armored within an adjacent inclusion of quartz, and matrix plagioclase, and (*ii*) M_{1c} garnet rims with nearby, but non-touching plagioclase and biotite (not included in Table 2). Prograde M_1 *P–T* conditions (~520ºC and 4.3 kbar; solid square symbol in Fig. 11) were calculated from armored plagioclase and biotite inclusions midway between the core and rim of a M_{1b} garnet porphyroblast.

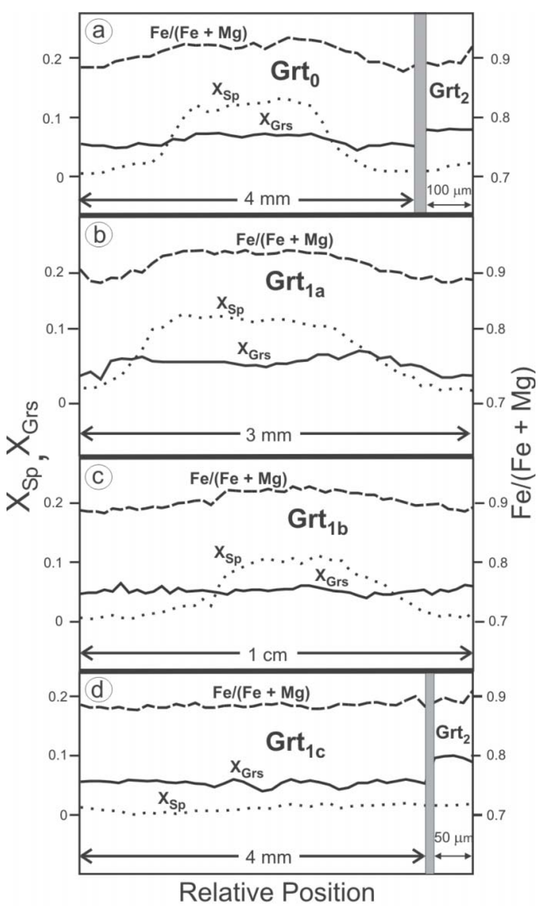

Fig. 10. Compositional profiles of garnet in z7635, described in text. a) M_0; (b) M_{1a}; (c) M_{1b}; (d) M_{1c}.

Phase-equilibrium relationships calculated from the bulk chemical composition of sample z7635 (Fig. 11) have a similar topology to those for z7641 (Fig. 7), except that garnet is stable over most of the diagram. The garnet-in boundary constrains the minimum M_0 temperature above 520ºC at ~4 kbar. The scant textural evidence for a pre-S_1 generation of staurolite (Table 3) suggests that M_0 temperatures may have reached ~540°C at ~4 kbar (Fig. 11). These temperature estimates are in good agreement with those based on the phase diagram for sample z7641 (Fig. 7). The clockwise M_1 *P–T*–t path derived from thermobarometric data for z7635 passes slightly above the aluminosilicate triple point, consistent with the predicted stability of M_1 garnet in sample z7635 (Fig. 11), as well as the instability of M_1 garnet predicted below ~4.5 kbar for z7641 (Fig. 7). The computed field of St + Grt + Bt + Pl + Qtz + H_2O stability and compositional isopleths agree well with the M_2 *P–T*–t path inferred on the basis of thermobarometric data for sample z7641.

Geochronology

Background

Direct dating of garnet and staurolite, utilizing ~10–50 mg separates, has been attempted with various isotopic systems, including Rb–Sr (Christensen *et al.* 1989, Vance & O'Nions 1992), U–Pb (Mezger *et al.* 1989, Burton & O'Nions 1991, Vance & O'Nions 1992, DeWolf *et al.* 1993), Pb–Pb (Lanzirotti & Hanson 1995, Frei *et al.* 1995) and Sm–Nd (Cohen *et al.* 1988, Vance & O'Nions 1990, Burton & O'Nions 1991, Argles *et al.* 1999, Vance *et al.* 1998b, Vance & Harris 1999, Prince *et al.* 2000, Jung & Mezger 2001). Results have provided constraints on *P–T*–t paths (*e.g.*, Mezger *et al.* 1989, Frei *et al.* 1995, Vance *et al.* 1998b, Vance & Harris 1999), the rate and duration of porphyroblast growth (Christensen *et al.* 1989, Burton & O'Nions 1991, Vance & O'Nions 1992, Vance & Harris 1999), and polymetamorphic histories *via* texturally and compositionally distinct portions of garnet porphyroblasts (Stowell & Goldberg 1997, Argles *et al.* 1999). With stepwise dissolution and *in situ* studies, investigators have documented the degree to which accessory micro-inclusions (*e.g.*, monazite, zircon, allanite) may dominate the the trace-element proportions in host porphyroblasts. Accordingly, care is required to ensure that bulk compositions are not compromised by accessory micro-inclusions that commonly occur in, but may be out of equilibrium with, the host porphyroblast (Vance & O'Nions 1992, Zhou & Hensen 1995, Frei *et al.* 1995, DeWolf *et al.* 1996, Vance *et al.* 1998a, Prince *et al.* 2000).

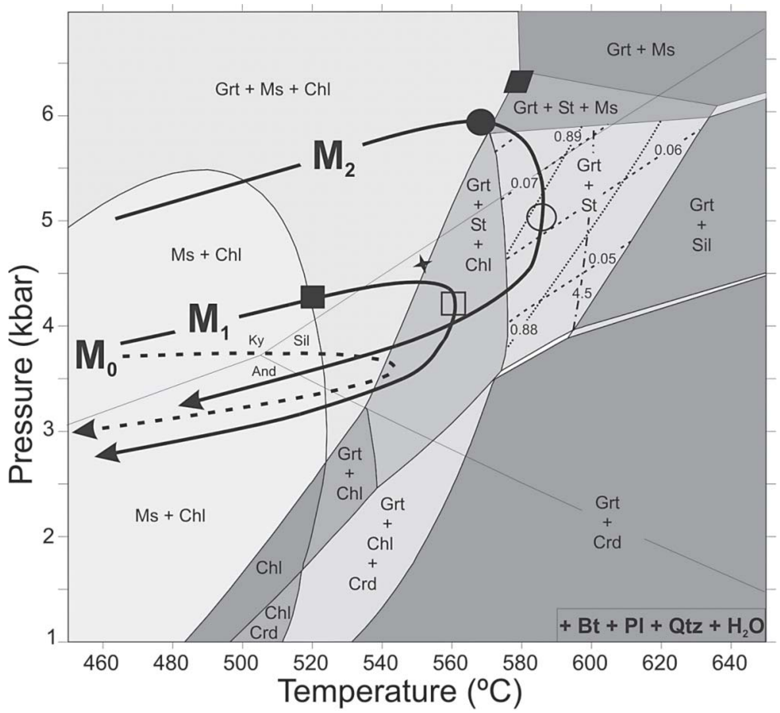

FIG. 11. Phase diagram calculated with the DOMINO software (De Capitani 1994) for sample z7635 (bulk composition in mole %: 67.20 SiO_2, 11.78 Al_2O_3, 7.90 FeO, 3.96 MgO, 3.90 CaO, 1.82 K_2O, 3.39 Na_2O, 0.07 MnO). All stability fields include Bt + Pl + Qtz + H_2O. See the caption of Figure 7 for details. Solid rhomb shows M_2 conditions based on average P–T results for sample z7635.

In situ geochronological techniques generally target inclusions of accessory minerals in porphyroblasts and, through preservation of both macroscopic and microscopic textural relationships, offer the potential to constrain the age of porphyroblasts, or texturally distinct cores and rims. These determinations can be compared with those from matrix minerals which, in polymetamorphic rocks, commonly yield the age of younger metamorphic events. Chemical dating of monazite with an electron microprobe was introduced as a low-cost, rapid means of reconnaissance-level *in situ* dating (Suzuki & Adachi 1991, Suzuki *et al.* 1994, Montel *et al.* 1996). Only recently have technical improvements (Scherrer *et al.* 2000, Williams *et al.* 1999, Pyle *et al.* 2002), combined with high-resolution X-ray (*e.g.*, Th, Y, U, Pb) map images of complexly zoned monazite (Williams *et al.* 1999), led to results that approach the precision achievable with sensitive high-resolution ion-microprobe (SHRIMP) analysis of zircon and monazite (DeWolf *et al.* 1993, Zhu *et al.* 1997, Foster *et al.* 2000, Montel *et al.* 2000, Stern & Berman 2000, Bosch *et al.* 2002, Catlos *et al.* 2002). In addition to its greater precision and accuracy, *in situ* SHRIMP dating of monazite, as applied in this paper, also allows the degree of concordancy of monazite analyses to be determined (Stern & Berman 2000).

A major challenge with *in situ* data is interpreting the significance of monazite inclusions in refractory porphyroblasts, such as garnet and staurolite. Given that these porphyroblasts offer excellent potential for shielding monazite inclusions from re-quilibration during younger events (DeWolf *et al.* 1993, Zhu *et al.* 1997, Montel *et al.* 2000, Stern & Berman 2000, Carson *et al.* 2004), the most conservative interpretation is that monazite inclusions in a porphyroblast provide a maximum age of porphyroblast growth. However, the possibility that inclusions may be pre-metamorphic (*i.e.*, detrital) or post-metamorphic (*e.g.*, secondary alteration) must also be considered. Stern & Berman (2000) suggested that the morphology of monazite inclusions in porphyroblasts could be used as a preliminary guide in interpreting the origin of monazite inclusions, be they detrital (xenoblastic grains with pronounced embayments might significantly pre-date porphyroblast growth), synchronous with porphyroblast growth (euhedral, compositionally simple grains with few or no embayments in planar grain-boundaries), or metamorphic or hydrothermal grains introduced *via* fractures transecting host grains (irregular, vermicular grains possibly associated with retrograde silicate minerals). Textural features of monazite must be used with caution, however, in light of recent studies that have demonstrated episodic growth and resorption of monazite, before and after garnet growth during a single metamorphic event (*e.g.*, Foster *et al.* 2002, Pyle & Spear 2003). The Y content of monazite has recently been used as a monitor of relative crystallization of monazite and garnet (*e.g.*, Pyle & Spear 1999, Foster *et al.* 2000, 2002, Pyle & Spear 2003). Although this technique has met with success in monocyclic metamorphic rocks, the generally complex compositional domains of even monocyclic grains of monazite (*e.g.*, Williams *et al.* 1999) compromise the utility of this technique in polymetamorphic rocks. Monazite–garnet thermometry, based on temperature-sensitive Y exchange (Pyle & Spear 2000), potentially offers a means of assessing whether monazite inclusions were in equilibrium with the host garnet, but more work is needed to assess the utility of this approach in polymetamorphic rocks. In this study, we illustrate how textural observations regarding the distribution of monazite inclusions within garnet may be used to demonstrate synchronous crystallization of monazite and garnet.

In situ analysis of porphyroblast inclusions also offers enormous potential in the dating of deformation events via porphyroblast–fabric relationships (Stern & Berman 2000, Berman *et al.* 2000a, 2002a, Williams & Jercinovic 2002, Carson *et al.* 2004). In general, where synchroneity of monazite and porphyroblast growth can be demonstrated, robust maximum and minimum ages of the fabric are obtained by dating monazite inclusions within a porphyroblast that is enveloped by the fabric, or cuts it, respectively. Direct dating of a deformation event is possible if it can be further demonstrated that porphyroblast growth and fabric development were contemporaneous. In addition, tectonic fabrics may be directly dated by microtextural observations, such as preferred orientations, geometries, and shapes of monazite grains and overgrowths (Williams & Jercinovic 2002; see below). This *in situ* method of dating deformation events is particularly important for metamorphic events at grades lower than upper-amphibolite, because synmetamorphic intrusive rocks may not be present to provide effective conventional geochronological brackets on the age of fabrics.

An important *caveat* in the interpretation of the significance of ages based on monazite inclusions stems from several studies that have demonstrated the partial or complete isotopic re-equilibration of inclusions that are connected to the matrix by fractures (DeWolf *et al.* 1993, Zhu *et al.* 1997, Montel *et al.* 2000, Carson *et al.* 2004). This process is likely due to efficient, fluid-mediated recrystallization, rather than diffusion, as the latter appears to be ineffective at temperatures below 900°C (Seydoux-Guillaume *et al.* 2002). The examples provided in the above studies underscore the need to anchor interpretations on a minimum of several "robust" inclusions not intersected by fractures, particularly because fractures that may have existed in the third dimension of a porphyroblast are not available for inspection.

Methods

Back-scattered electron (BSE) images of *in situ* monazite grains were acquired on a Cambridge S360 (located at Geological Survey of Canada, Ottawa, and operating at 20 kV accelerating voltage and 2 nA beam current) in order to assess internal structure, facilitate selection of analytical sites, and provide further insight into the petrological context.

U–Pb analyses were performed *in situ* on monazite using the SHRIMP II located at the Geological Survey of Canada facility in Ottawa, Canada. Analytical protocols for monazite have been previously described in detail (Stern & Berman 2000). Selected monazite targets within 3–5 mm cores of thin sections were prepared for *in situ* analysis according to the methods of Rayner & Stern (2002). A small plug of pre-polished laboratory standard monazite (GSC monazite z3345; $^{207}Pb/^{206}Pb$ TIMS age = 1821.0 ± 0.6 Ma (2σ), Stern & Berman 2000) was included in both mounts. Analyses were conducted using an O_2^- primary beam. Two different spot-sizes were used during the analyses, with diameters of 16 and 12 μm and beam currents of *ca.* 0.7 and 0.3 nA, respectively. The count rates of ten isotopes of Ce^+, U^+, Th^+, and Pb^+ were sequentially measured over seven scans with a single electron multiplier and a pulse-counting system with deadtime of 24 ns. Moderate filtering of energy was used to eliminate a known isobar at mass 204 (Stern & Berman 2000). Off-line data processing was accomplished using customized in-house software. The 1σ external errors of $^{206}Pb/^{238}U$ ratios reported in the data tables incorporate a ±1.0–1.2% error in calibrating the standard monazite. The program ISOPLOT (Ludwig 2001) was used to generate Concordia plots and weighted mean ages. Error ellipses are shown on all Concordia diagrams at the 1σ level, whereas weighted mean $^{207}Pb/^{206}Pb$ ages quoted in the text are at the 95% confidence level.

Results

X-ray maps (Y, Th, U, Ca), obtained with a Cameca SX50 electron microprobe at the University of Massachusetts, Amherst (*e.g.*, Williams *et al.* 1999), show that all monazite grains discussed below are characterized by single age domains, with the exception of a <5 μm rim that was not analyzed on one matrix grain (z7635–117).

Sample z7641

Analyses of three different elongate inclusions of high-Y monazite ~10 × 30–90 μm within M_{1b} (Figs.

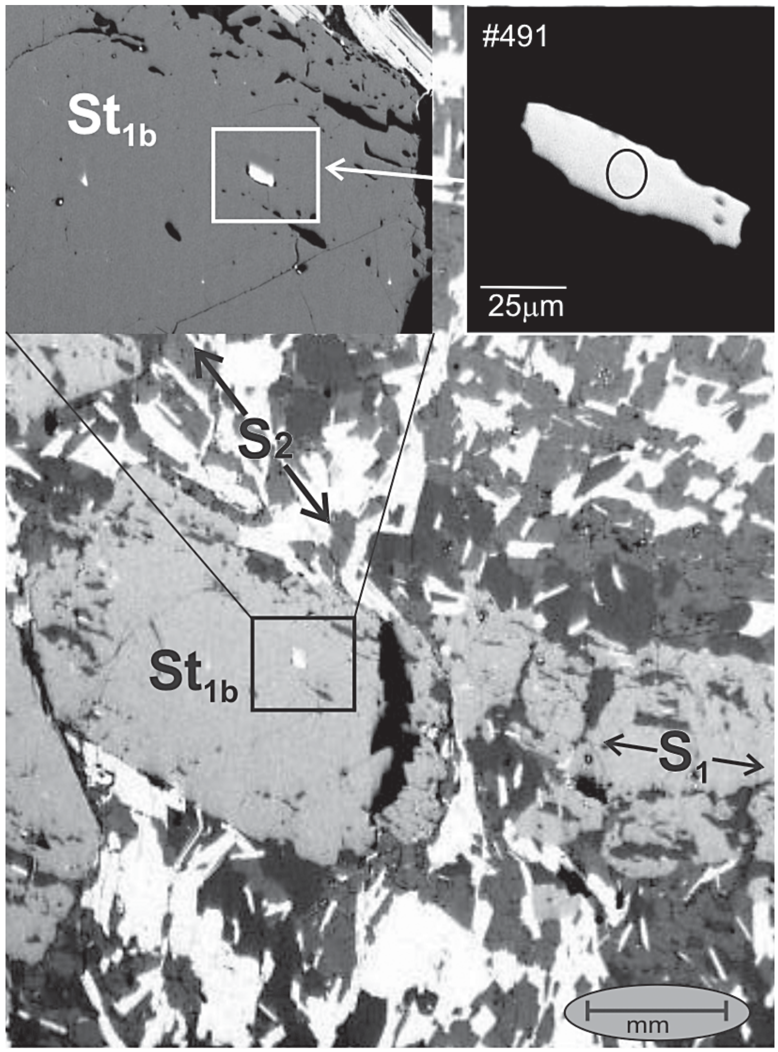

FIG. 12. SEM images of elongate, *ca.* 2.34 Ga monazite inclusion (#491) in M_{1b} staurolite of z7641. Note that monazite forms part of the included S_1 fabric that is only very weakly preserved in the matrix, and that monazite also contains slightly elongate S_1 inclusions of quartz.

5a, 12) and M_2 (Fig. 5c) staurolite porphyroblasts yield a weighted mean $^{207}Pb/^{206}Pb$ age of 2342 ± 9 Ma (mean squares of weighted deviates (MSWD) = 0.29, probability of fit (POF) = 0.75; filled ellipses in Fig. 13a; Table 4). Four analyses of three, low-Y monazite grains from the matrix yield a weighted mean $^{207}Pb/^{206}Pb$ age of 1837 ± 10 Ma (MSWD = 0.80; POF = 0.49; filled ellipses in Fig. 13b; Table 4). The latter include a ~20 × 30 μm subhedral grain of monazite along grain boundaries of S_2-parallel (monazite #206; Table 4) and randomly oriented (monazite #207) biotite. The third grain of matrix monazite (monazite #492) is ~40 × 60 μm, irregular, and interstitial to two porphyroblasts of M_1 staurolite.

At an early stage of this study, reconnaissance chemical ages of monazite were obtained with an JEOL 6400 electron microprobe at Carleton University, Ottawa, for several small (<10 μm) targets in this sample. Analyses fall into *ca.* 2.3 and 1.8 Ga age clusters with a precision of approximately 0.05 Ga. One of the *ca.* 1.8 Ga analyses was obtained for a 8 × 10 μm monazite inclusion (not intersected by fractures) near the rim of a post-S_2 (M_2) garnet porphyroblast.

Sample z7635

Monazite occurs as large (up to 100 μm long), low-Y grains in the matrix and as small, high-Y inclusions in M_1 garnet (<30 μm in M_{1b}, <10 μm in M_{1c}). Three partly rounded to irregular, ~20 μm inclusions of monazite were analyzed from two M_{1b} garnet porphyroblasts (Fig. 14a). None of the three grains are associated with any detectable fractures within the host garnet. Four analyses yield a weighted mean $^{207}Pb/^{206}Pb$ age of 2347 ± 9 Ma (MSWD = 1.11; POF = 0.34; open ellipses in Fig 13a; Table 4). Monazite inclusions in M_{1c} garnet were considered too small for precise SHRIMP analysis. Four grains of low-Y monazite on grain boundaries of S_2-parallel biotite also were analyzed. These are subhedral, elongate (100 × 50 μm, monazite #117, Table 4; Fig. 14b) to rounded, equant grains between 20 and 30 μm in diameter (monazite #118, #130 and #131). Frayed edges (#117, #130 and #131) are common. Ten analyses from these four grains yield a weighted mean $^{207}Pb/^{206}Pb$ age of 1839 ± 6 Ma (MSWD = 0.88; POF = 0.55; open ellipses in Fig. 13b).

Discussion

Interpretation of new geochronological results

Geochronological data for samples z7641 and z7635 point to two episodes of monazite growth, at *ca.* 2.34 and 1.84 Ga (Fig. 13). The tight clusters defining these

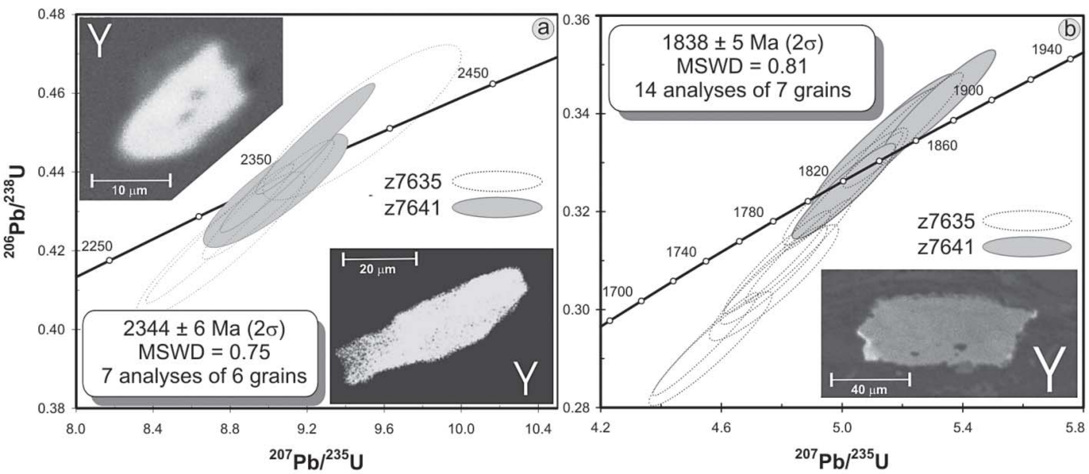

FIG. 13. Concordia plots of GSC SHRIMP II U–Pb data for *in situ* monazite. (a) Age determinations of *ca.* 2.34 Ga monazite inclusions with X-ray maps of yttrium showing uniformly high levels of Y in inclusions of *ca.* 2.34 Ga monazite in garnet (upper left) and staurolite (lower right). (b) Age determinations of *ca.* 1.84 Ga matrix monazite, with X-ray map of yttrium for a representative low-Y grain in the matrix (except for the rim).

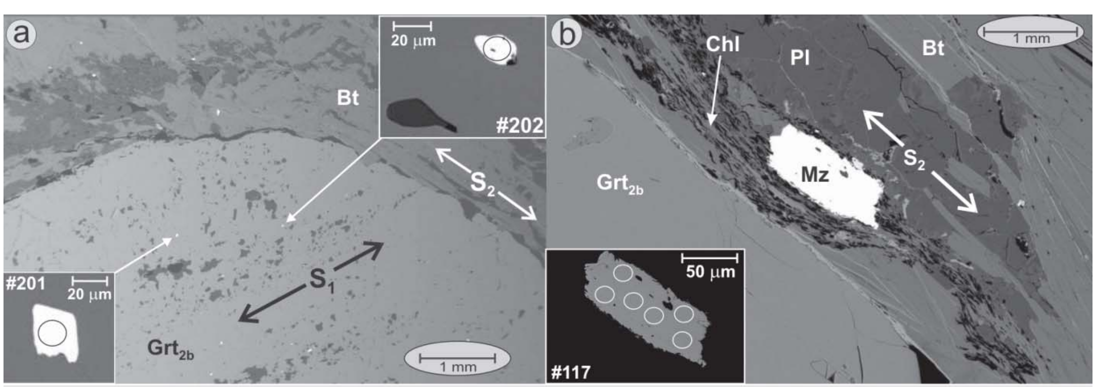

FIG. 14. SEM images of monazite in z7635: (a) *ca.* 2.34 Ga inclusions in M_{1b} garnet, (b) grain of *ca.* 1.84 Ga monazite in the matrix.

TABLE 4. SHRIMP U-Pb IN SITU MONAZITE DATA FOR SAMPLES z7641 and z7635

spot name	Spot	Isotopic ratios								Apparent ages (Ma)						
		Th/U	$^{204}Pb/^{206}Pb$	$^{207}Pb/^{235}U$	± $^{207}/_{235}$	$^{206}Pb/^{238}U$	± $^{206}/_{238}$	$^{207}Pb/^{206}Pb$	± $^{207}/_{206}$	$^{206}Pb/^{238}U$	± $^{206}/_{238}$	$^{207}Pb/^{235}U$	± $^{207}/_{235}$	$^{207}Pb/^{206}Pb$	± $^{207}/_{206}$	% concor-dance
7641-104.1	M_1S	15.1	0.000038	9.035	0.153	0.4354	0.0059	0.1505	0.0013	2330	26	2342	16	2351.5	14.9	99.1
7641-491.1	M_1S	10.3	0.000033	9.059	0.128	0.4388	0.0057	0.1497	0.0006	2345	26	2344	13	2342.9	6.6	100.1
7641-302.1	M_2S	10.8	0.000023	9.242	0.127	0.4486	0.0057	0.1494	0.0006	2389	26	2362	13	2339.5	6.3	102.1
7641-207.1	mat	11.1	0.000032	5.006	0.069	0.3236	0.0040	0.1122	0.0006	1807	19	1820	12	1835.0	9.5	98.5
7641-492.1	mat	14.2	0.000036	5.319	0.077	0.3414	0.0044	0.1130	0.0006	1894	21	1872	12	1847.8	9.2	102.5
7641-206.1	mat	9.2	0.000051	5.148	0.095	0.3339	0.0055	0.1118	0.0007	1857	27	1844	16	1829.0	11.6	101.6
7641-206.2	mat	9.9	0.000055	5.120	0.090	0.3322	0.0051	0.1118	0.0008	1849	25	1839	15	1828.3	12.3	101.1
7635-116.1	M_2G	12.7	0.000026	8.744	0.157	0.4246	0.0072	0.1494	0.0006	2281	33	2312	17	2338.7	6.8	97.5
7635-116.2	M_2G	10.5	0.000019	9.486	0.211	0.4527	0.0080	0.1520	0.0017	2407	36	2386	21	2368.2	19.6	101.7
7635-201.1	M_2G	15.4	0.000032	8.997	0.140	0.4332	0.0062	0.1506	0.0007	2320	28	2338	14	2353.2	8.1	98.6
7635-202.1	M_2G	16.2	0.000037	8.747	0.180	0.4216	0.0076	0.1505	0.0012	2268	34	2312	19	2351.2	13.6	96.5
7635-118.1	mat	9.5	0.000017	4.857	0.072	0.3119	0.0043	0.1129	0.0004	1750	21	1795	13	1847.1	7.0	94.8
7635-118.2	mat	8.1	0.000040	4.547	0.071	0.2930	0.0043	0.1126	0.0004	1656	21	1740	13	1841.2	7.2	90.0
7635-117.1	mat	9.5	0.000046	4.785	0.072	0.3097	0.0043	0.1121	0.0005	1739	21	1782	13	1833.1	8.3	94.9
7635-117.2	mat	10.1	0.000035	5.011	0.085	0.3251	0.0049	0.1118	0.0007	1815	24	1821	14	1828.5	11.1	99.2
7635-117.3	mat	10.1	0.000032	5.202	0.081	0.3366	0.0048	0.1121	0.0005	1870	23	1853	13	1833.4	8.7	102.0
7635-117.4	mat	10.0	0.000035	4.773	0.072	0.3071	0.0041	0.1127	0.0006	1726	20	1780	13	1843.9	10.2	93.6
7635-117.5	mat	9.3	0.000029	5.004	0.080	0.3242	0.0049	0.1119	0.0004	1810	24	1820	14	1831.2	6.9	98.9
7635-117.6	mat	10.2	0.000042	6.085	0.177	0.3956	0.0098	0.1116	0.0014	2149	45	1988	26	1824.8	23.1	117.8
7635-131.1	mat	10.5	0.000044	4.774	0.087	0.3055	0.0048	0.1133	0.0008	1719	24	1780	15	1853.5	13.4	92.7
7635-130.1	mat	14.0	0.000062	4.564	0.083	0.2921	0.0048	0.1133	0.0007	1652	24	1743	15	1853.7	11.8	89.1

Notes: Concordance = 100 x ($^{206}Pb/^{238}U$ age)/($^{207}Pb/^{206}Pb$ age). Uncertainties listed as 1σ and include all known sources of error (Stern & Berman, 2000). Data have been corrected for common Pb according to procedures outlined in (Stern & Berman, 2000). One sigma uncertainties derived from calibrations of monazite standard (z3345) are 1.2% (z7635) and 1.0% (z7641).

Spot abbreviations: mat=matrix; M_1S, M_2S, M_2G = inclusions in M_1 staurolite, M_2 staurolite, or M_2 garnet two age populations, the single-age-domain X-ray maps of the analyzed monazite, and the lack of evidence for fractures intersecting the monazite grains analyzed, argue against any significant amount of disturbance of these isotopic ages. Thus we consider that these data reflect monazite growth during two discrete metamorphic events that affected the southwestern CBb. We examine below the linkages between these two age clusters and the metamorphic and structural features of these samples, correlations which establish a *ca.* 2.34 Ga age for M_1 at a late stage of penetrative D_1 deformation, and a *ca.* 1.84 Ga age for M_2 at a late stage of penetrative D_2 deformation (Table 5).

The M_1 event is dated at 2344 ± 6 Ma (MSWD = 0.75; POF = 0.61) on the basis of the weighted mean $^{207}Pb/^{206}Pb$ age of seven analyses of monazite inclusions within staurolite and garnet porphyroblasts. These inclusions are mainly situated within M_{1b} garnet (z7635) and M_{1b} staurolite (z7641), both interpreted as late- to post-D_1 porphyroblasts. Although accessory inclusions (*e.g.*, monazite, zircon) typically yield the maximum age of the host grain, the distribution of monazite within z7635 garnet types further establishes a link between the growth of *ca.* 2.34 Ga monazite and M_{1b} garnet. Monazite inclusions were not observed in M_0 or M_{1a} garnet, and are restricted to the outer 1 mm of M_{1b} garnet rims (*e.g.*, Fig. 8d). In contrast, they occur throughout M_{1c} garnet (Fig. 8e). These differences suggest that *ca.* 2.34 Ga monazite growth began during a temporal progression from M_{1a} to M_{1c} garnet, consistent with the relatively high contents of yttrium in these monazite inclusions within garnet (*e.g.*, Foster *et al.* 2002, Pyle & Spear 2003). Thermobarometric results point to increasing temperature during this progression, suggesting operation of a temperature-sensitive monazite-growth reaction (*e.g.*, Ferry 2000, Foster *et al.* 2000, 2002, Pyle & Spear 2003, Wing *et al.* 2003, Kohn & Malloy 2004) during prograde growth of the M_{1b} garnet. In sample z7635, monazite formation is pinned between 520°C, the temperature of the garnet-in boundary (Fig. 11), and 560°C, the peak temperature determined by thermobarometry (Table 2, Fig. 11). This temperature range is compatible with linkage of monazite growth to the staurolite-in reaction (~540°C; Fig. 11), as concluded elsewhere (Kohn & Malloy 2004).

The interpretation of a *ca.* 2.34 Ga age for prograde M_1 growth of staurolite, garnet, and monazite at a late stage of D_1 is reinforced by textural features in z7641. Two elongate, *ca.* 2.34 Ga monazite inclusions in M_{1b} staurolite (Figs. 5a, 12) in part define $S_{internal}$ that is parallel to $S_{external}$ (S_1) and also to the elongation of staurolite porphyroblasts, thereby supporting syn- to late-tectonic growth of both staurolite and monazite during the D_1 event at *ca.* 2.34 Ga. The relatively high Y content of the *ca.* 2.34 Ga monazite inclusions in staurolite is also compatible with monazite crystallization prior to growth of the M_2 garnet. One elongate inclusion of monazite, also dated at *ca.* 2.34 Ga, is enclosed by a post-D_2 (M_2) staurolite porphyroblast that overgrows the reworked S_1 foliation (Fig. 5c). These relationships are interpreted to reflect growth of *ca.* 2.34 Ga monazite during D_1, with subsequent D_2 deformation and overgrowth by post-D_2 staurolite. Evidence that M_2 staurolite and garnet porphyroblastesis was late- to post-D_2 (Tables 1, 3) allows the possibility that reworking of S_1 and reorientation of this *ca.* 2.34 Ga monazite grain, which does not display a younger overgrowth, occurred at an early stage of D_2, when the temperature may have been below that required for growth of M_2 monazite.

A younger metamorphic event is dated at 1838 ± 5 Ma (MSWD = 0.81; POF = 0.66), the weighted mean $^{207}Pb/^{206}Pb$ age of 14 analyses of matrix monazite in samples z7641 and z7635. Monazite dated at *ca.* 1.84 Ga occurs both as elongate crystals on grain boundaries with S_2-aligned biotite, and as equant grains intergrown with randomly oriented matrix biotite. This textural range suggests that growth *ca.* 1.84 Ga monazite was syn- to post-D_2, consistent with the timing of M_2 porphyroblasts in both rocks. Similarly, the occurrence of both high- and low-Y monazite in the matrix in z7641 is compatible with monazite growth both synchronously

TABLE 5. TIME-CORRELATED METAMORPHIC AND DEFORMATION SEQUENCE FOR THE SOUTHWESTERN COMMITTEE BAY BELT

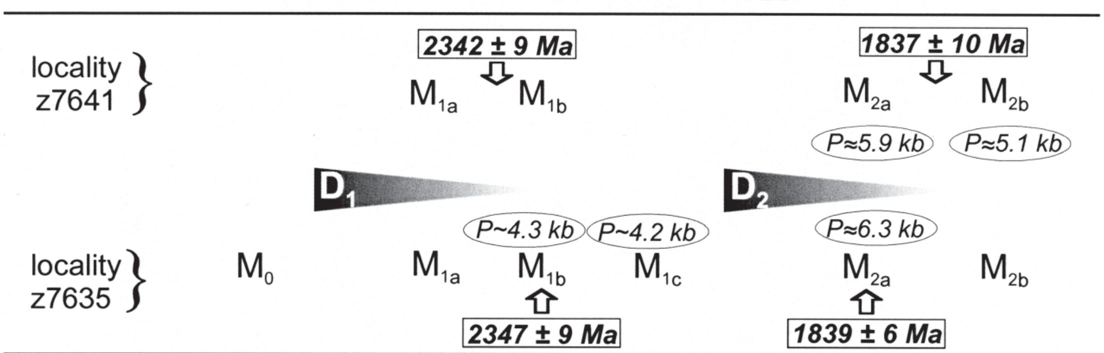

with, and after, growth of M_2 garnet. A lower limit on penetrative D_2 strain at this locality is provided by the *ca.* 1.8 Ga CHIME age of a monazite inclusion in post-S_2 garnet in z7641. S_2 is also constrained in the Laughland Lake area to pre-date *ca.* 1820 Ma, the age of an unstrained monzogranite dyke that cuts penetrative S_2 fabrics in the Walker Lake intrusive complex (Skulski *et al.* 2003b).

In summary, structural, metamorphic, and geochronological data from rocks of the southwestern CBb reflect the impact of two discrete tectonometamorphic events, at *ca.* 2.34 and 1.84 Ga. The M_1 event is associated with S_1 development in a low-P regime with estimated near-peak *P–T* conditions of ~4.2 kbar and 560°C. Thermobarometric data and calculated phase diagrams indicative of a clockwise *P–T*–t path (Figs. 7, 11), and the association of D_1 fold and fabric development with syn- to post-S_1 staurolite (z7635 and z7641) and garnet (z7635) growth, are characteristic of metamorphism in response to crustal shortening and thickening. This interpretation is compatible with the presence of inclined west-verging F_1 folds and a possible west-vergent D_1 thrust in this area (Fig. 2).

In an analogous fashion, M_2 garnet and staurolite growth (z7635 and z7641) occurred late- to post-D_2 at *ca.* 1.84 Ga in a relatively low-P regime. M_2 achieved a maximum pressure of ~6.1 kbar (average results of samples z7635 and z7641) on a clockwise *P–T*–t path that produced post-D_2 growth of andalusite in adjacent rocks during decompression (Figs. 7, 11). This metamorphic event is also attributed to crustal shortening leading to thickening, as manifested by regional-scale, northwest-vergent F_2 folds with mainly SE-dipping axial planes. The inference of two episodes of crustal thickening is further indicated by the absence of plutonic rocks that could have provided an alternative source of heat immediately prior to, or during, the *ca.* 2.34 and *ca.* 1.84 Ga events.

Sample z7635 and andalusite-rich metapelite at locality 3_{And} exhibit scant textural evidence for a cryptic, pre-S_1 metamorphic event that is not reflected in our monazite data. We consider it likely that this event reflects regional contact metamorphism at *ca.* 2.58 Ga, a time of widespread and voluminous plutonism within the CBb (Skulski *et al.* 2003b), and the age of the low-(Th/U) rim on *ca.* 2.61–2.60 Ga magmatic zircon in plutonic rocks across the CBb (Skulski *et al.* 2002b). We do not see evidence for a metamorphic event prior to *ca.* 2.58 Ga or for deformation earlier than *ca.* 2.35 Ga; we cannot rule out the possibility of such earlier Neoarchean tectonometamorphic events, however.

Comparison between southwestern PAg subdomain and northern migmatite subdomain

A broader perspective on the tectonometamorphic evolution of the Committee Bay region can be achieved through comparison of these new results with recent data from the northern migmatite domain (locality 5; Fig. 2; Carson *et al.* 2004). There, low-*P* (~5 kbar), upper-amphibolite-facies (640–680ºC) migmatitic paragneiss and metatexite–diatexite exhibit a first-generation gneissosity (S_1) that is largely overprinted by, or completely transposed into, an east-trending biotite–sillimanite S_2 schistosity. Results of *in situ* SHRIMP analyses of monazite from selected samples fall into three distinct age-populations: *ca.* 2.35 ± 0.01, 1.85 ± 0.01, and 1.78 ± 0.01 Ga. In part on the basis of imprecisely defined *ca.* 2.3 Ga U–Pb ages of zircon within concordant leucosome and paleosome, Carson *et al.* (2004) tentatively suggested that low-*P*, D_1 migmatization took place at *ca.* 2.35 Ga in the northern migmatite subdomain, in accord with our new results implicating a *ca.* 2.34 Ga tectonometamorphic event in the southwestern part of the CBb. Also in agreement with our new results, Carson *et al.* (2004) determined that garnet porphyroblasts and the enveloping S_2 fabric formed between *ca.* 1.85 Ga, the age of the monazite inclusions in garnet, and *ca.* 1.815 Ga, the age of a post-tectonic monzogranite dyke that cut S_2 within the northern migmatite subdomain (M. Sanborn-Barrie, unpubl. data).

The overall agreement between data from the northern migmatite and southwestern PAg subdomains provide compelling evidence for two regional episodes of low-*P* metamorphism and deformation at *ca.* 2.35 Ga and *ca.* 1.85 Ga (the average ages based on data from both subdomains). The absence within the CBb of pre- to syn-2.35 Ga or -1.85 Ga plutonic rocks that could have provided heat implies that both metamorphic events occurred in response to episodes of shortening (D_1 and D_2) accompanied by modest thickening of the crust. An interesting feature of the comparison between subdomains is that both record similar structural levels during M_2 (~5–6 kbar), but temperatures were ~100°C hotter in the northern migmatite subdomain. The same relationship appears to hold for M_1, although M_1 *P–T* conditions are less well defined in the northern migmatite subdomain. Available radiometric data (Holman *et al.* 2001) suggest that these lateral thermal gradients may have been produced by the higher heat-productivity of the sedimentary-rock-dominated northern migmatite subdomain relative to the volcanic-rock-dominated southwestern PAg (Berman *et al.* 2003; in prep.).

A ca. 2.35 Ga tectonothermal event: local or regional significance?

Complementary datasets for the northern migmatite subdomain (Carson *et al.* 2004) and the southwestern PAg subdomain (this paper) reveal that the CBb experienced an important tectonometamorphic event at around 2.35 Ga (D_1, M_1). A major question is whether this newly recognized tectonometamorphic event is restricted to the CBb, or whether it is of regional significance in the Rae domain. Metamorphic zones in the CBb are distributed such that M_1 metamorphic grade increases toward the north and northwest (Fig. 2). Geochronology is very limited in most of the area inferred to be at higher grade, with geological control outside the CBb provided only from helicopter surveys using eight-km grid stations (Heywood 1967). One exception is an upper-amphibolite-facies Grt–Bt–Sil paragneiss (Q, Fig. 1), collected during grid mapping of the Queen Maud block, and investigated during the course of a metamorphic compilation of the western Churchill Province (Berman *et al.* 2000b). Chemical monazite ages determined at the University of Massachusetts, Amherst (Williams *et al.* 1999) for this sample fall into four clusters: 2.52 ± 0.01 Ga from garnet-core inclusions, 2.41 ± 0.01 Ga from garnet-rim inclusions, 2.38 ± 0.01 Ga from the moderate-Y core of a matrix grain (Fig. 15), and 2.35 ± 0.01 Ga from the low-Y rim of the same matrix grain (Fig. 15). This sample preserves a record of distinct pulses of monazite growth at this locality, which, given the lack of low-grade assemblages or retrogression in this rock, likely reflect mid- to upper-amphibolite-facies metamorphic events. They also provide a maximum age of *ca.* 2.41 Ga for the development of a tectonic fabric, which wraps garnet at this locality. The youngest age-cluster corresponds well with ages determined in the CBb, providing evidence that other parts of the northern Rae domain experienced metamorphism at *ca.* 2.35 Ga.

Additional evidence for early Paleoproterozoic tectonic activity in the Rae domain can be found in ages of plutonic rocks, ages of metamorphism, and detrital ages in sedimentary rocks (*e.g.*, Aspler & Chiarenzelli 1998, McNicoll *et al.* 2000). Early Paleoproterozoic plutonism is manifest in widespread *ca.* 2.4–2.3 Ga granitic rocks located in both the southwestern and northern Rae domain (Fig. 1). For instance, in the Beaverlodge area of northwestern Saskatchewan (Bl, Fig. 1), granitic gneisses record ages between 2.4 and 2.3 Ga (Tremblay *et al.* 1981, Van Schmus *et al.* 1986, Hartlaub *et al.* 2003). Granitic gneiss in Archean basement rocks of the Taltson magmatic zone, north of 60°N (Tn, Fig. 1), range in age between 2.44–2.33 Ga (five samples) and 2.29–2.27 Ga (two samples; Bostock *et al.* 1991, van Breemen *et al.* 1992). Within the Taltson basement complex south of 60°N (Ts, Fig. 1), granitic and mafic gneiss range between 2.39 and 2.30 Ga (five samples), and a syenogranite gneiss is 2.14 Ga in age (McNicoll *et al.* 2000). Magmatic rocks of the Buffalo Head terrane on the west flank of the Taltson magmatic zone (Fig. 1) are characterized by slightly younger ages (Villeneuve *et al.* 1993) of *ca.* 2.32–2.0 Ga. In the Thelon tectonic zone, U–Pb zircon ages of tonalite – granitic gneiss are *ca.* 2.30 Ga north of the MacDonald fault (Th, Fig. 1; Roddick & van Breemen 1994) and *ca.* 2.48, 2.32, and 2.20 Ga on southern Boothia Peninsula (B, Fig. 1; Frisch & Hunt 1993).

In addition to this widespread *ca.* 2.4–2.0 Ga plutonic activity, a *ca.* 2.4–2.3 Ga record is apparent in ages of detrital zircon from sedimentary sequences distributed over a wide part of the Rae and Hearne domains. Some examples include (Fig. 1): the Lake Harbour group on southern Baffin Island (Scott *et al.* 2002), the Piling Group in central Baffin Island (Wodicka *et al.* 2003), the Goulbourn Group of the eastern Slave Province (McCormick *et al.* 1989), and the Murmac Bay group in northwestern Saskatchewan (O'Hanley *et al.* 1994). Presently, the best-studied example is the upper Hurwitz Group, which is characterized by a prominent *ca.* 2.35–2.31 Ga mode of detrital zircon (Davis *et al.* 2000).

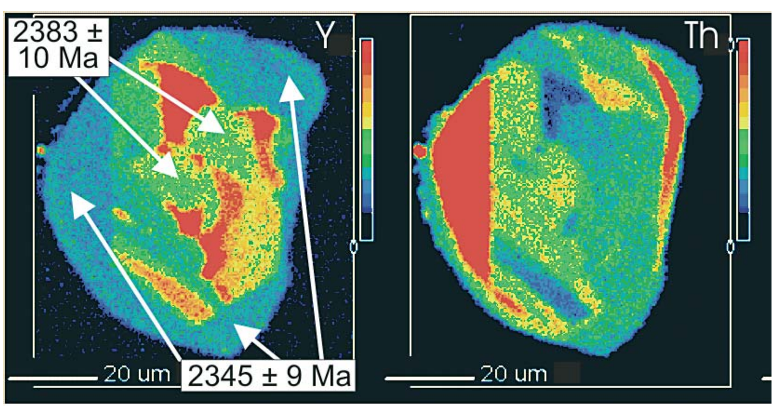

FIG. 15. X-ray maps of Y and Th distribution, collected at the University of Massachusetts, Amherst, showing *ca.* 2.38 and 2.35 Ga age domains in matrix monazite from Queen Maud paragneiss sample 60–TJ–382. Each quoted age represents the mean result of 9–10 spot analyses taken from the two domains indicated with arrows.

Metamorphic ages of *ca.* 2.4–2.3 Ga have also been reported from other parts of the Rae domain and from within the Snowbird tectonic zone. At Angikuni Lake (Fig. 1), multi-grain analyses of titanite in K-feldspar megacrystic granodiorite have been interpreted to indicate a *ca.* 2.35 Ga tectonometamorphic event (MacLachlan *et al.*, in prep.). In the Chesterfield Inlet segment of the Snowbird tectonic zone, a high-pressure (~12 kbar, 870°C) gabbro on the south flank of Kramanituar complex (Fig. 1) yielded a *ca.* 2.32 Ga age on multi-grain titanite, suggestive of high-*P* metamorphism at that time (Sanborn-Barrie *et al.* 2001). High-*P* granulite-facies rocks in the East Athabasca (southwestern) segment of the Snowbird tectonic zone also contain local evidence for *ca.* 2.4 Ga monazite (Williams *et al.* 1999). Further southwest in the Clearwater complex south of the Athabasca basin, *in situ* SHRIMP geochronology of agmatitic anorthosite has been interpreted to indicate a cryptic *ca.* 2.3 Ga metamorphic event (Crocker *et al.* 1993).

Tectonic implications

The presence of 2.4–2.0 Ga granitic gneiss within the Archean basement rocks of the Taltson magmatic zone led to the postulation of a continental arc formed during east-dipping subduction beneath the western margin of the Rae domain (Hoffman 1990, Ross *et al.* 1991, Bostock & van Breemen 1994). Aspler & Chiarenzelli (1998) considered that the absence of a linear distribution of *ca.* 2.5–2.0 Ga magmatic rocks was inconsistent with an arc environment, and instead suggested that the plutonism was anorogenic, having formed during a protracted period of *ca.* 2.5–2.1 Ga extension that ultimately led to rifting of a late Archean supercontinent (Kenorland). However, if one considers the spatial relationship of *ca.* 2.4–2.3 Ga localities that have been dated in the southwestern Rae domain, the Queen Maud block, and on southern Boothia Peninsula (Fig. 1), a linear distribution emerges that is on the same scale as, and parallel to, the Taltson magmatic zone and the Thelon tectonic zone. Accordingly, we consider that existing data are permissive, if not suggestive, of a *ca.* 2.4–2.3 Ga continental arc. An important test of this concept would be provided by geochronological investigations in a large, poorly understood region lying between the Taltson basement rocks straddling 60°N latitude and the McDonald fault (M; Fig. 1). The existence of a continental arc along the western margin of the Rae domain could provide a mechanism to account for *ca.* 2.4–2.35 Ga tectonometamorphism in the Queen Maud and Committee Bay regions, during which west-directed F_1 folds and thrusts led to crustal thickening (M_1 in this study). In this scenario, deformation, crustal thickening, and subsequent metamorphism would be far-field effects of subduction and arc magmatism in a tectonic setting akin to the modern-day Andean environment, where convergence between Nasca and South American plates has created a fold-and-thrust belt that presently extends up to 700 km from the trench (*e.g.*, Mueller *et al.* 2002). However, the focused time of tectonometamorphism in the CBb (*ca.* 2.35 Ga), metamorphism in the Queen Maud block (*ca.* 2.35 Ga), and of much of the magmatism reported in the western Rae domain (*ca.* 2.4–2.3 Ga), is consistent with collisional orogenesis following ocean closure and cessation of arc magmatism. A test of this model would be whether geochemical data support a transition from *ca.* 2.4 Ga subduction-related magmatism to *ca.* 2.3 Ga crustal melts generated in a syn- to post-collisional setting. Preliminary evidence indicates that *ca.* 2.3 Ga plutonic rocks in the Beaverlodge area are consistent with a collisional origin (Hartlaub *et al.* 2003).

McNicoll *et al.* (2000) presented Nd isotopic data for *ca.* 2.4–2.1 Ga granitic gneisses of the Taltson basement complex as well as undated mafic amphibolites. On the basis of $\varepsilon_{Nd(2.2\ Ga)}$ values up to +3.9, the latter were considered to represent mantle-derived melts formed during the *ca.* 2.45–2.1 Ga period of extension favored by Aspler & Chiarenzelli (1998). The most convincing geological evidence for extension in the Rae domain is provided by the *ca.* 2.08 Ga age of the Rutledge River basin (Bostock & van Breemen 1994) and a mafic magmatic event at *ca.* 2.19 Ga (Tulemalu – MacQuoid dyke swarm; Fahrig *et al.* 1984, Tella *et al.* 1997, W. Davis & A. LeCheminant, unpubl. data) to *ca.* 2.15 Ga (Shultz Lake gabbro; A. LeCheminant, unpubl. data). Bostock & van Breemen (1994) hypothesized a short-lived extensional event at *ca.* 2.34 Ga, the age assigned to the Thoa gabbro in Taltson basement complex, but the significance of this age is currently considered uncertain (H. Bostock, pers. commun., 2003). Accordingly, we suggest that an extensional environment was not initiated in the Rae domain until after *ca.* 2.35 Ga, the time of crustal shortening and thickening, and may not have been significant until *ca.* 2.19 Ga, when mafic magmatism potentially associated with rifting took place prior to the assembly of Laurentia after *ca.* 2.0 Ga (Hoffman 1988).

The northwest-vergent D_2 structures and associated low-*P* M_2 metamorphism of the CBb characterize a broad region of the central Rae domain, including the Neoarchean Woodburn Lake group, and the Paleoproterozoic Amer and Chantrey groups (see Fig. 1; Sanborn-Barrie *et al.* 2002, Carson *et al.* 2004). The northeast orientation of D_2 fabrics, together with new geochronological constraints, led Carson *et al.* (2004) to suggest that crustal thickening was a far-field response to Trans-Hudson orogenic events. Given the ~20–30 Ma time lag between the onset of crustal thickening and metamorphism predicted by thermal models (*e.g.*, England & Thompson 1984, Jamieson *et al.* 1998, Huerta *et al.* 1999), *ca.* 1.85 Ga tectonometamorphism, as dated in the CBb, was likely a response to collisional events that preceded the *ca.* 1.86–1.85 Ga magmatism that led to the Wathaman and Cumberland batholiths.

Accretionary events at *ca.* 1.88–1.86 Ga (Bickford *et al.* 1990, Corrigan *et al.* 2003, Tran *et al.* 2003) on the southern Hearne margin (suture #1 in Fig. 1) provide one far-field mechanism to drive shortening in the Rae domain (*cf.* Carson *et al.* 2004). However, a more compelling spatial context is provided by the possibility of an early collisional event involving a microcontinent, such as the Hudson "protocontinent" (see Fig. 1), postulated on the basis of geophysical data (Roksandic *et al.* 1987), or the Meta Incognita terrane (Sanborn-Barrie *et al.* 2004). The latter has been identified through field and associated geochronological studies on Baffin Island (St-Onge *et al.* 2002), and is suggested to have accreted with the northeastern Rae domain at *ca.* 1.88–1.86 Ga (suture #2 in Fig. 1; St-Onge, pers. commun. 2004).

Summary and Conclusions

New constraints on the Paleoproterozoic evolution of the Rae domain are provided by structural, metamorphic, and *in situ* geochronological data from the southwestern part of the Archean Committee Bay belt. Our main findings are as follows:

1) two deformational events (D_1, D_2) reflect compressional tectonics involving west- to northwest-directed folds and possible thrusts;

2) porphyroblast growth occurred primarily during two metamorphic events, with M_1 and M_2 occurring syn- to post-D_1 and syn- to post-D_2, respectively;

3) late- to post-D_1 growth of staurolite and garnet (M_1) is dated at 2344 ± 6 Ma, at a late stage of D_1 strain on a clockwise P–T–t path passing through ~4.3 kbar and 520°C prior to near-peak conditions of 4.2 kbar and 560°C;

4) M_2 occurred at 1838 ± 5 Ma, at a late stage of D_2 strain on a clockwise P–T–t path passing through ~5.9 kbar and 570°C, prior to decompression to 5.1 kbar and 585°C and late growth of andalusite;

5) isolated textural observations suggest an early thermal event that may correspond to regional contact metamorphism induced by *ca.* 2.6–2.58 Ga granitic plutonism (Skulski *et al.* 2003b).

These new data accord well with a similar dataset from the northern migmatite subdomain (Carson *et al.* 2004), and together indicate that the CBb experienced *ca.* 2.35 and 1.85 Ga tectonometamorphic events in a relatively low-P regime. Petrological evidence for clockwise P–T–t paths, porphyroblast growth that is late- to post-tectonic with respect to compressional fabrics, and the absence of known intrusive rocks with ages that immediately predate, or are synchronous with M_1 and M_2, collectively suggest that the heat source for both metamorphic events was not magmatic, but related to radiogenic heating in response to crustal thickening. As proposed for some Australian low-P terranes (*cf.* Sandiford & Hand 1998, Sandiford *et al.* 1998), the occurrence of Archean granitic rocks in the CBb with anomalously high heat-productivity (Holman *et al.* 2001) suggests that low-P metamorphism in the CBb may have been the consequence of moderate degrees of thickening involving radiogenically enriched crustal components (Berman *et al.* 2003).

The compressional forces that produced modest thickening events across the CBb at *ca.* 2.35 Ga and *ca.* 1.85 Ga are envisaged to be associated with reworking of the western Churchill upper plate during two far-field orogenic events. We suggest that the first event may have involved *ca.* 2.35 Ga collisional orogenesis following continental arc magmatism along the western margin of the Rae domain. This interpretation is consistent with Hoffman's (1990) initial suggestion of an early Paleoproterozoic continental arc and Stockwell's (1982) inference of an orogenic event (early phase of his "Blezardian" orogeny) based on a *ca.* 2.32 Ga age (zircon upper intercept) for a Taltson basement gneiss. In view of the general restriction of the term "Blezardian" in literature of the last decade to an orogenic event in the Superior Province (*e.g.*, Siddorn & Halls 2002), we refer to the *ca.* 2.35 Ga event in the Rae domain as the "Arrowsmith" orogeny (after a prominent river in the northern migmatite subdomain that was named by the Arctic explorer, John Rae, after the famous British mapmaker, John Arrowsmith). Regionally significant evidence for a 2.35 Ga collisional event may impact on models for the initiation of Hurwitz Group sedimentary rocks, presently considered to have accumulated in response to early Paleoproterozoic lithospheric extension (Aspler *et al.* 2001, Berman *et al.* 2004). In addition to providing a potential source for abundant *ca.* 2.3 Ga detrital zircon in the upper Hurwitz Group (Davis *et al.* 2005), arc magmatism on the western flank of the Rae domain may also fill an apparent gap in the generation of juvenile continental crust at this time (Condie *et al.* 2001). We consider that *ca.* 1.85–1.84 Ga tectonometamorphism was linked to an early, *ca.* 1.88–1.86 Ga accretionary stage of the Trans-Hudson orogen involving microcontinents such as the Hudson "protocontinent" or the Meta Incognita terrane.

New insights obtained into the early Paleoproterozoic evolution of the Rae domain highlight the utility of linked structural, metamorphic, and *in situ* geochronological analysis to unravel polymetamorphic and polydeformational histories. Whereas this *in situ* methodology offers a major contextual advantage over direct dating of porphyroblasts separated from rocks, this benefit can be offset by the uncertainty of whether porphyroblasts and analyzed inclusions of monazite grew during the same metamorphic event. We illustrate in this paper how porphyroblast–fabric relationships combined with textural features, such as the distribution of inclusions of monazite within porphyroblasts and preferred shape of some monazite inclusions and their host porphyroblasts, may be used to better establish a direct link between fabric development, porphyroblast crystallization, and monazite growth.

Acknowledgements

First and foremost, we thank Dugald Carmichael for his immense contribution in reminding us during every encounter that appreciation of the beauty of nature is paramount, not only for its inherent value but also as a critical requirement in inspiring us to challenge our models until they ultimately approach the truth. The work summarized in this paper could not have been undertaken without the full support and encouragement provided by participants of the Committee Bay TGI project, especially its co-leaders Tom Skulski and Hamish Sandeman. We gratefully acknowledge insight into the regional geology of this area gained through initial work by H. Sandeman, C. Studnicki-Gizbert and J. Brown, who collected one of the samples (z7641) utilized in this study. We thank Katherine Venance for carrying out the electron-microprobe analyses, Maggie Currie for SEM and drafting assistance, Pat Hunt for providing X-ray maps and help with SEM operation, Nicole Rayner for assistance with SHRIMP work, Mike Jercinovic for obtaining high-resolution chemical ages on monazite and X-ray maps, Doug Tinkham for kindly sharing datafiles used in preliminary THERMOCALC calculations, Tom Hoisch for providing pressure estimates using his calibration of equilibrium (3), Christian de Capitani for assistance with DOMINO queries, and Robert F. Martin for his important role as editor of this paper and this special volume. We are also grateful for very thorough and constructive reviews provided by Vicki McNicoll, Nicole Rayner, Tom Skulski, Marc St-Onge, Mike Williams, and Natasha Wodicka. This is GSC contribution number 2003223.

References

ANSDELL, K.M., LUCAS, S.B., CONNORS, K. & STERN, R.A. (1995): Kisseynew metasedimentary gneiss belt, Trans-Hudson Orogen (Canada); back-arc origin and collisional inversion. *Geology* **23**, 1039-1043.

ARGLES, T.W., PRINCE, C.I., FOSTER, G.L. & VANCE, D. (1999): New garnets for old? Cautionary tales from young mountain belts. *Earth Planet. Sci. Lett.* **172**, 301-309.

ASHTON, K.E. (1981): Preliminary report on geological studies of the "Woodburn Lake Group" northwest of Tehek Lake, District of Keewatin. *Geol. Surv. Can., Curr. Res.* **81-1A**, 269-273.

ASPLER, L.B. & CHIARENZELLI, J.R. (1997): Initiation of ~2.45–2.1 Ga intracratonic basin sedimentation of the Hurwitz Group, Keewatin hinterland, Northwest Territories, Canada. *Precamb. Res.* **81**, 265-297.

________ & ________ (1998): Two Neoarchean supercontinents? Evidence from the Paleoproterozoic. *Sediment. Geol.* **120**, 75-104.

________, ________ & COUSENS, B.L. (2004) Fluvial, lacustrine, and volcanic sedimentation in the Angikuni subbasin, and initiation of ~1.84–1.79 Ga Baker Lake Basin, western Churchill Province, Nunavut, Canada. *Precamb. Res.* **129**, 225-250.

________, WISOTZEK, I.E., CHIARENZELLI, J.R., LOSONCZY, M.F., COUSENS, B.L., MCNICOLL, V.J. & DAVIS, W.J. (2001): Paleoproterozoic intracratonic basin processes, from breakup of Kenorland to assembly of Laurentia: Hurwitz Basin, Nunavut, Canada. *Sediment. Geol.* **141–142**, 287-318.

BELL, R.T. (1970): The Hurwitz group; a prototype for deposition on metastable cratons. *In* Precambrian Basins and Geosynclines of the Canadian Shield (A.J. Baer, ed.). *Geol. Surv. Can., Pap.* **70–40**, 159-169.

BERMAN, R.G. (1991): Thermbarometry using multiequilibrium calculations: a new technique with petrological applications. *Can. Mineral.* **29**, 833-855.

________ & ARANOVICH, L.Y. (1996): Optimized standard state and mixing properties of minerals. I. Model calibration for olivine, orthopyroxene, cordierite, garnet, and ilmenite in the system $FeO–MgO–CaO–Al_2O_3–TiO_2–SiO_2$. *Contrib. Mineral. Petrol.* **126**, 1-24.

________, ________ & RANCOURT, P. (1995): Phase equilibrium constraints on the stability of biotite. 2. Fe–Al biotite in the system $K_2O–FeO–Al_2O_3–SiO_2–H_2O–CO_2$. *Geol. Surv. Can., Curr. Res.* **1995–E**, 263-270.

________, CARSON, C.J., SANBORN-BARRIE, M., SKULSKI, T., STERN, R. & RAYNER, N. (2003): New constraints on polymetamorphism in the Committee Bay belt, Rae domain, with implications for the tectonometamorphic history of the Western Churchill province. *Geol. Assoc. Can. – Mineral. Assoc. Can., Program Abstr.* **28**.

________, DAVIS, W.J., ASPLER, L. & CHIARENZELLI, J.R. (2002b): SHRIMP U/Pb ages of multiple metamorphic events in the Angikuni Lake area, western Churchill Province, Nunavut. *Geol. Surv. Can., Curr. Res.* **2002–F3**, 1-9.

________, ________, RYAN, J.J. & TELLA, S. (2002a): *In situ* U/Pb SHRIMP geochronology of Barrovian facies-series metasedimentary rocks in the Happy Lake and Josephine River supracrustal belts: implications for the Paleoproterozoic architecture of the northern Hearne domain, Nunavut. *Geol. Surv. Can., Curr. Res.* **2002–F4**, 1-14.

________, EASTON, R.M. & NADEAU, L. (2000b): A new tectonometamorphic map of the Canadian Shield; introduction. *In* Tectonometamorphic Studies in the Canadian Shield (Part II). *Can. Mineral.* **38**, 277-286.

________, RYAN, J.J., TELLA, S., SANBORN-BARRIE, M., STERN, R., ASPLER, L., HANMER, S. & DAVIS, W. (2000a): The case of multiple metamorphic events in the Western Churchill Province: evidence from linked thermobarometric and *in situ* SHRIMP data, and jury deliberations. *Geosci. Can., Summit Meeting 2000, Abstr.* 836.

________, SANBORN-BARRIE, M., STERN, R., JERCINOVIC, M. & SKULSKI, T. (2004): Collisional orogenesis at *ca.* 2.35 Ga in the Rae domain, western Churchill Province, Nunavut, Canada. *Geol. Soc. Am., Abstr. Program*

Bickford, M.E., Collerson, K.D., Lewry, J.F., Van Schmus, W.R. & Chiarenzelli, J.R. (1990): Proterozoic collisional tectonism in the Trans-Hudson Orogen, Saskatchewan. *Geology* **18**, 14-18.

Bosch, D., Hammor, D., Bruguier, O., Caby, R. & Luck, J.-M. (2002): Monazite "in situ" $^{207}Pb/^{206}Pb$ geochronology using a small geometry high-resolution ion probe: application to Archaean and Proterozoic rocks. *Chem. Geol.* **184**, 151-165.

Bostock, H.H. & Van Breemen, O. (1994): Ages of detrital and metamorphic zircons and monazites from a pre-Taltson magmatic zone basin at the western margin of the Rae Province. *Can. J. Earth Sci.* **31**, 1353-1364.

________, ________ & Loveridge, W.D. (1991): Further geochronology of plutonic rocks in northern Taltson Magmatic Zone, District of Mackenzie, N.W.T. *In* Radiometric Age and Isotopic Studies. Report 4. *Geol. Surv. Can., Curr. Res.* **90–2**, 67-78.

Brown, M. (2002): Retrograde processes in migmatites and granulites revisited. *J. Metamorph. Geol.* **20**, 25-40.

Burton, K.W. & O'Nions, R.K. (1991): High-resolution garnet chronometry and the rates of metamorphic processes. *Earth Planet. Sci. Lett.* **107**, 649-671.

Carson, C.J., Berman, R.G. & Stern, R.A. (2002): An *in situ* U–Pb geochronological study of high-grade gneisses flanking the Committee Bay granite–greenstone belt: implications for the tectonothermal history of the Rae Province. *Geol. Assoc. Can. – Mineral. Assoc. Can., Program Abstr.* **27**, 18.

________, ________, ________, Sanborn-Barrie, M., Skulski, T. & Sandeman, H.A.I. (2004): Age constraints on the Paleoproterozoic tectonometamorphic history of the Committee Bay region, western Churchill Province, Canada: evidence from zircon and *in situ* monazite SHRIMP geochronology. *Can. J. Earth Sci.* **41**, 1049-1076.

Catlos, E.J., Harrison, T.M., Manning, C.E., Grove, M., Rai, S.M., Hubbard, M.S. & Upreti, B.N. (2002): Records of the evolution of the Himalayan Orogen from *in situ* Th–Pb ion microprobe dating of monazite; eastern Nepal and western Garhwal. *J. Asian Earth Sci.* **20**, 459-479.

Christensen, J.N., Rosenfeld, J.L. & DePaolo, D.J. (1989): Rates of tectonometamorphic processes from rubidium and strontium isotopes in garnet. *Science* **244**, 1465-1469.

Cohen, A.S., O'Nions, R.K., Siegenthaler, R. & Griffin, W.L. (1988): Chronology of the pressure–temperature history recorded by a granulite terrain. *Contrib. Mineral. Petrol.* **98**, 303-311.

Condie, K.C., Des Marais, D.J. & Abbott, D. (2001): Precambrian superplumes and supercontinents; a record in black shales, carbon isotopes, and paleoclimates? *Precamb. Res.* **106**, 239-260.

Corrigan, D., MacHattie, T.G. & Chakungal, J. (2003): Paleoproterozoic crustal evolution, with particular emphasis on the Trans-Hudson Orogen and bounding Archean cratons. *Geol. Assoc. Can. – Mineral. Assoc. Can., Program Abstr.* **28**, 695.

Crocker, C.H., Collerson, K.D., Lewry, J.F. & Bickford, M.E. (1993): Sm–Nd, U–Pb, and Rb–Sr geochronology and lithostructural relationships in the southwestern Rae Province: constraints on crustal assembly in the western Canadian Shield. *Precamb. Res.* **61**, 27-50.

Davis, W.J., Hanmer, S., Aspler, L., Sandeman, H., Tella, S., Zaleski, E., Relf, C., Ryan, J., Berman, R.G. & MacLachlan, K. (2000): Regional differences in the Neoarchean crustal evolution of the Western Churchill Province: can we make sense of it? *Geosci. Can., Summit Meeting 2000, Abstr.* 864.

________, Rainbird, R.H., Aspler, L. & Chiarenzelli, J.R. (2005): Detrital zircon geochronology of the Paleoproterozoic Hurwitz and Kiyuk groups, western Churchill Province. *In* Radiometric Age and Isotopic Studies. Report 18. *Geol. Surv. Can., Curr. Res.* **2005–F** (in press).

De Capitani, C. (1994): Gleichgewichts-Phasendiagramme: Theorie und Software. *Ber. Deutsch. Mineral. Gesellsch.* **72**, 48 (abstr.).

DeWolf, C.P., Belshaw, N.S. & O'Nions, R.K. (1993): A metamorphic history from micron-scale $^{207}Pb/^{206}Pb$ chronometry of Archean monazite. *Earth Planet. Sci. Lett.* **120**, 207-220.

________, Zeissler, C.J., Halliday, A.N., Mezger, K. & Essene, E.J. (1996): The role of inclusions in U–Pb and Sm–Nd garnet geochronology: stepwise dissolution experiments and trace uranium mapping by fission track analysis. *Geochim. Cosmochim. Acta* **60**, 121-134.

England, P.C. & Thompson, A.B. (1984): Pressure–temperature–time paths of regional metamorphism. I. Heat transfer during the evolution of regions of thickened continental crust. *J. Petrol.* **25**, 894-928.

Essene, E.J. (1989): The current status of thermobarometry in metamorphic rocks. *In* Evolution of Metamorphic Belts (J.S. Daly, R.A. Cliff & B.W.D. Yardley, eds.). *Geol. Soc., Spec. Publ.* **43**, 1-44.

Fahrig, W.F., Christie, K.W., Eade, K.E. & Tella, S. (1984): Paleomagnetism of the Tulemalu Dykes, Northwest Territories, Canada. *Can. J. Earth Sci.* **21**, 544-553.

Ferry, J.M. (2000): Patterns of mineral occurrence in metamorphic rocks. *Am. Mineral.* **85**, 1573-1588.

Foster, G., Gibson, H.D., Parrish, R., Horstwood, M., Fraser, J. & Tindle, A. (2002): Textural, chemical and isotopic insights into the nature and behaviour of metamorphic monazite. *In* Chemistry and Physics of Accessory Minerals; Crystallization, Transformation and Geochronological Applications. *Chem. Geol.* **191**, 183-207.

________, Kinny, P., Vance, D., Prince, C. & Harris, N. (2000): The significance of monazite U–Th–Pb age data in metamorphic assemblages; a combined study of monazite and garnet chronometry. *Earth Planet. Sci. Lett.* **181**, 327-340.

Fraser, J.A. (1988): Geology of the Woodburn Lake map area, District of Keewatin. *Geol. Surv. Can., Pap.* **87–11**.

FREI, R., BIINO, G.G. & PROSPERT, C. (1995): Dating a Variscan pressure–temperature loop with staurolite. *Geology* **23**, 1095-1098.

FRISCH, T. (1982): Precambrian geology of the Prince Albert Hills, western Melville Peninsula, Northwest Territories. *Geol. Surv. Can., Bull.* **346**.

________ & HUNT, P.A. (1993): U–Pb zircon and monazite ages from the Precambrian Shield of Ellesmere and Devon islands, Arctic Archipelago. *In* Radiogenic Age and Isotopic Studies, Report 2. *Geol. Surv. Can., Curr. Res.* **93–2**, 3-22.

GIBB, R.A. & WALCOTT, R.I. (1971): A Precambrian suture in the Canadian Shield. *Earth Planet. Sci. Lett.* **10**, 417-422.

GUIRAUD, M., POWELL, R. & REBAY, G. (2001): H_2O in metamorphism and unexpected behaviour in the preservation of metamorphic mineral assemblages. *J. Metamorph. Geol.* **19**, 445-454.

HARTLAUB, R.P., HEAMAN, L.M., CHACKO, T., ASHTON, K.E. & CREASER, R.A. (2003): Episodic crustal reworking in the Rae Province of northern Saskatchewan: evidence from integrated field, isotopic and geochemical data. *Geol. Assoc. Can. – Mineral. Assoc. Can., Program Abstr.* **28**, 659.

HENDERSON, J.B., JAMES, D.T. & THOMPSON, P.H. (1999): Geology, Healey Lake – Artillery Lake, Northwest Territories – Nunavut. *Geol. Surv. Can., Open File* **3819**.

________, THOMPSON, P. & JAMES, D. (1982): The Healey Lake map area and the Thelon Front problem, District of Mackenzie. *Geol. Surv. Can., Curr. Res.* **82–01A**, 191-195.

HEYWOOD, W.W. (1967): Geological notes, northeastern District of Keewatin and southern Melville Peninsula, District of Franklin, Northwest Territories. *Geol. Surv. Can., Pap.* **66–40**, 1-22.

HOFFMAN, P.F. (1988): United plates of America, the birth of a craton: Early Proterozoic assembly and growth of Laurentia. *Annu. Rev. Earth Sci.* **16**, 543-603.

________ (1990) Subdivision of the Churchill Province and extent of the Trans-Hudson Orogen. *In* The Early Proterozoic Trans-Hudson Orogen of North America (J.F. Lewry & M.R. Stauffer, eds.). *Geol. Assoc. Can., Spec. Pap.* **37**, 15-39.

HOISCH, T.D. (1990): Empirical calibration of six geobarometers for the mineral assemblage quartz + muscovite + biotite + plagioclase + garnet. *Contrib. Mineral. Petrol.* **104**, 225-234.

HOLLAND, T.J.B. & POWELL, R. (1998): An internally consistent thermodynamic data set for phases of petrological interest. *J. Metamorph. Geol.* **16**, 309-343.

HOLMAN, P.B., CARSON, J.M., FORD, K.L., GRANT, J.A. & SHIVES, R.B.K. (2001): Airborne gamma ray spectrometry compilation series, Quoich River, Nunavut. *Geol. Surv. Can., Open File* **4005**.

HUERTA, A.D., ROYDEN, L.H. & HODGES, K.V. (1999): The effects of accretion, erosion and radiogenic heat on the metamorphic evolution of collisional orogens. *J. Metamorph. Geol.* **17**, 349-366.

JACKSON, G.D. (1966): Geology and mineral possibilities of the Mary River region, northern Baffin Island. *Can. Mining J.* **87**, 57-61.

________ (2000): Geology of the Clyde–Cockburn land map area, north-central Baffin Island, District of Franklin. *Geol. Surv. Can., Mem.* **440**.

JAMIESON, R.A., BEAUMONT, C., FULLSACK, P. & LEE, B. (1998): Barrovian regional metamorphism; where's the heat? *In* What Drives Metamorphism and Metamorphic Reactions? (P.J. Treloar & P.J. O'Brien, eds.). *Geol. Soc., Spec. Publ*. **138**, 23-51.

JOHNSTONE, S. (2002): *Structural and Geochronological Constraints on the Tectonic Evolution of the Walker Lake Area, Committee Bay Belt, Nunavut*. M.Sc. thesis, Univ. Waterloo, Waterloo, Ontario.

________, LIN, S. & SANDEMAN, H. (2002): Significance of the Walker Lake shear Zone with respect to regional deformation in the Committee Bay belt, central mainland, Nunavut. *Geol. Surv. Can., Curr. Res.* **2002–C15**, 1-11.

JUNG, S. & MEZGER, K. (2001): Geochronology in migmatites; a Sm–Nd, U–Pb and Rb–Sr study from the Proterozoic Damara Belt (Namibia): implications for polyphase development of migmatites in high-grade terranes. *J. Metamorph. Geol.* **19**, 77-97.

KOHN, M.J. & MALLOY, M.A. (2004): Formation of monazite via prograde metamorphic reactions among common silicates: implications for age determinations. *Geochim. Cosmochim. Acta* **68**, 101–113.

KRETZ, R. (1983): Symbols for rock-forming minerals. *Am. Mineral.* **68**, 277-279.

LANZIROTTI, A. & HANSON, G.N. (1995): U–Pb dating of major and accessory minerals formed during metamorphism and deformation of metapelites. *Geochim. Cosmochim. Acta* **59**, 2513-2526.

LECHEMINANT, A.N., RODDICK, J.C., TESSIER, A.C. & BETHUNE, K.M. (1987): Geology and U–Pb ages of early Proterozoic calc-alkaline plutons northwest of Wager Bay, District of Keewatin. *Geol. Surv. Can., Curr. Res.* **87–1A**, 773-782.

LUDWIG, K.R. (2001): *User's Manual for Isoplot/Ex rev. 2.49: a Geochronological Toolkit for Microsoft Excel*. Berkeley Geochronology Center, Berkeley, California (Spec. Publ. 1a).

MACHATTIE, T. (2002): Physical volcanology of komatiites in the Laughland and Walker Lake areas, Committee Bay belt, Nunavut. *Geol. Surv. Can., Curr. Res.* **2002–C14**, 1-9.

MACLACHLAN, K., RELF, C., DAVIS, W.J. & ASPLER, L. (1999): U/Pb geochronological constraints on Archean and Proterozoic deformation: Yathkyed–Angikuni area, western Churchill Province. *27th Yellowknife Geoscience Forum,* 40-41.

McCormick, D.S., Bowring, S.A. & Grotzinger, J.P. (1989): Geochronology, provenance evolution, and correlation in foreland basins using volcanic and detrital zircons; the early Proterozoic Goulburn Supergroup, Kilohigok Basin, Canada. *Geol. Soc. Am., Abstr. Program* **21**, A373.

McNicoll, V.J., Thériault, R.J. & McDonough, M.R. (2000): Taltson basement gneissic rocks; U–Pb and Nd isotopic constraints on the basement to the Paleoproterozoic Taltson magmatic zone, northeastern Alberta. *Can. J. Earth Sci.* **37**, 1575-1596.

Meyer, M.T., Bickford, M.E. & Lewry, J.F. (1992): The Wathaman Batholith: an early Proterozoic continental arc in the Trans-Hudson orogenic belt, Canada. *Geol. Soc. Am., Bull.* **104**, 1073-1085.

Mezger, K., Hanson, G.N. & Bohlen, S.R. (1989): U–Pb systematics of garnet: dating the growth of garnet in the late Archean Pikwitonei granulite domain at Cauchon and Natawahunan lakes, Manitoba, Canada. *Contrib. Mineral. Petrol.* **101**, 136-148.

Montel, J.-M., Foret, S., Veschambre, M., Nicollet, C. & Provost, A. (1996): Electron microprobe dating of monazite. *Chem. Geol.* **131**, 37-53.

________, Kornprobst, J. & Vielzeuf, D. (2000): Preservation of old U–Th–Pb ages in shielded monazite: example from the Beni Bousera Hercynian kinzigites (Morocco). *J. Metamorph. Geol.* **18**, 335-342.

Mueller, J., Kley, J. & Jacobshagen, V. (2002): Structure and Cenozoic kinematics of the Eastern Cordillera, southern Bolivia (21°S). *Tectonics* **21**, doi:10.1029/2001tc001340.

O'Hanley, D.S., Kyser, T.K. & Sibbald, T.I.I. (1994): The age and origin of the North Shore plutons in the Rae Province, Goldfields area, Saskatchewan. *Can. J. Earth Sci.* **31**, 1397-1406.

Pattison, D.R.M. (1992): Stability of andalusite and sillimanite and the Al_2SiO_5 triple point: constraints from the Ballachulish aureole, Scotland. *J. Geol.* **100**, 423-446.

Peterson, T.D., Van Breemen, O., Sandeman, H. & Cousens, B. (2002): Proterozoic (1.85–1.75 Ga) igneous suites of the Western Churchill Province: granitoid and ultrapotassic magmatism in a reworked Archean hinterland. *Precamb. Res.* **119**, 73-100.

Pouchou, J.L. & Pichoir, F. (1985): PAP correction procedure for improved quantitative microanalysis. *In* Microbeam Analysis (J.T. Armstrong, ed.). San Francisco Press, San Francisco, California (104-106).

Prince, C.I., Kosler, J., Vance, D. & Günther, D. (2000): Comparison of laser ablation ICP–MS and isotope dilution REE analyses; implications for Sm–Nd garnet geochronology. *Chem. Geol.* **168**, 255-274.

Pyle, J.M. & Spear, F.S. (1999): Yttrium zoning in garnet: coupling of major and accessory phases during metamorphic reactions. *Am. Mineral.* **88**, 708.

________ & ________ (2000): An empirical garnet (YAG) – xenotime thermometer. *Contrib. Mineral. Petrol.* **138**, 51-58.

________ & ________ (2003): Four generations of accessory-phase growth in low-pressure migmatites from SW New Hampshire. *Am. Mineral.* **88**, 338-351.

________, ________, Wark, D.A., Kohn, M.J., Rakovan, J. & Hughes, J.M. (2002): Electron microprobe analysis of REE in apatite, monazite and xenotime; protocols and pitfalls. *In* Phosphates: Geochemical, Geobiological, and Materials Importance (M.L. Kohn, J. Rakovan & J.M. Hughes, eds.). *Rev. Mineral. Geochem.* **48**, 337-362.

Rainbird, R.H., Hadlari, T., Aspler, L.B., Donaldson, J.A., LeCheminant, A.N. & Peterson, T.D. (2003): Sequence stratigraphy and evolution of the Paleoproterozoic intracontinental Baker Lake and Thelon basins, western Churchill Province, Nunavut, Canada. *Precamb. Res.* **125**, 21-53.

Rayner, N. & Stern, R.A. (2002): Improved sample preparation method for SHRIMP analysis of delicate mineral grains exposed in thin sections. *Geol. Surv. Can., Curr. Res.* **2002–F10**, 1-3.

Roddick, J.C. & Van Breemen, O. (1994): U–Pb zircon dating: a comparison of ion microprobe and single grain conventional analyses. *In* Radiogenic Age and Isotopic Studies, Report 8. *Geol. Surv. Can., Curr. Res.* **1994–F**, 1-9.

Roksandic, M.M., Beaumont, C. & Tankard, A.J. (1987): The tectonics and evolution of the Hudson Bay region. *Atlantic Geosci. Soc., Spec. Publ.* **5**, 507-518.

Ross, G.M., Parrish, R.R., Villeneuve, M.E. & Bowring, S.A. (1991): Geophysics and geochronology of the crystalline basement of the Alberta Basin, western Canada. *Can. J. Earth Sci.* **28**, 512-522.

Sanborn-Barrie, M., Berman, R.G., Skulski, T., Sandeman, H., Carson, C. & Rayner, N. (2004): Is main-stage *ca.* 1.85–1.82 Ga tectonometamorphism of the Committee Bay belt, Rae domain, western Churchill Province, a far-field (upper-plate) expression of Trans-Hudson orogenesis? *In* From Forelands to Core Zones: Deformation and Tectonic Evolution of Orogenic Belts; a conference and field trip in honour of Dr. Philip Simony, p. 43.

________, Carr, S.D. & Thériault, R. (2001): Geochronological constraints on metamorphism, magmatism, and exhumation of deep-crustal rocks of the Kramanituar Complex, with implications for the Paleoproterozoic evolution of the Archean western Churchill Province, Canada. *Contrib. Mineral. Petrol.* **141**, 592-612.

________, Sandeman, H., Skulski, T., Brown, J., MacHattie, T., Deyell, C., Carson, C., Panagapko, D. & Byrne, D. (2003): Structural geology of the northeastern Committee Bay belt, Ellice Hills area, central Nunavut. *Geol. Surv. Can., Curr. Res.* **2003–C23**, 1-13.

________, Skulski, T., Sandeman, H., Berman, R.G., Johnstone, S., MacHattie, T. & Hyde, D. (2002): Structural and metamorphic geology of the Walker Lake – Arrowsmith River area, Committee Bay belt, Nunavut. *Geol. Surv. Can., Curr. Res.* **2002–C12**, 1-13.

SANDEMAN, H.A., BROWN, J., GREINER, E., HYDE, D., JOHNSTONE, S., MACHATTIE, T., STUDNICKI-GIZBERT, C. & PLAZA, D. (2002): Geology, Laughland Lake, Nunavut. *Geol. Surv. Can., Open File* **4190** (scale 1:100 000, 2 sheets).

________, ________, STUDNICKI-GIZBERT, C., MACHATTIE, T., HYDE, D., JOHNSTONE, S., GREINER, E. & PLAZA, D. (2001a): Bedrock mapping in the Committee Bay belt, Laughland Lake area, central mainland, Nunavut. *Geol. Surv. Can., Curr. Res.* **2001–C12**, 1-20.

________, DAVIS, W., HANMER, S., MACLACHLAN, K., RYAN, J., KJARSGAARD, B., KERSWILL, J., TELLA, S., ZALESKI, E., COUSENS, B. & RELF, C. (2000): Archean volcanic sequences of the Western Churchill Province, Nunavut, Canada: three petrochemically distinct domains of non-plateau affinity. *Geosci. Canada, Summit Meeting 2000*.

________, SKULSKI, T. & SANBORN-BARRIE, M. (2004): Geology, Ellice Hills, Nunavut. *Geol. Surv. Can., Open File* **1794** (scale 1:100 000, 2 sheets).

________, STUDNICKI-GIZBERT, C., BROWN, J. & JOHNSTONE, S. (2001b): Regional structural and metamorphic geology of the Committee Bay Belt, Laughland Lake area, central mainland, Nunavut. *Geol. Surv. Can., Curr. Res.* **2001–C13**, 1-13.

SANDIFORD, M. & HAND, M. (1998): Australian Proterozoic high-temperature, low-pressure metamorphism in the conductive limit. *In* What Drives Metamorphism and Metamorphic Reactions? (P. Treloar & P.J. O'Brien, eds.). *Geol. Soc., Spec. Publ.* **138**, 103-114.

________, ________ & MCLAREN, S. (1998): High geothermal gradient metamorphism during thermal subsidence. *Earth Planet. Sci. Lett.* **163**, 149-165.

SCHAU, M. (1978): Metamorphism of the Prince Albert group, District of Keewatin. *In* Metamorphism in the Canadian Shield (J.A. Fraser & W.W. Heywood, eds.). *Geol. Surv. Can., Pap.* **78–10**, 203-213.

________ (1982): Geology of the Prince Albert group in parts of Walker Lake and Laughland Lake map areas, District of Keewatin. *Geol. Surv. Can., Bull.* **337**.

SCHERRER, N.C., ENGI, M., GNOS, E., JAKOB, V. & LIECHTI, A. (2000): Monazite analysis; from sample preparation to microprobe age dating and REE quantification. *Schweiz. Mineral. Petrogr. Mitt.* **80**, 93-105.

SCOTT, D.J., STERN, R.A., ST-ONGE, M.R. & MCMULLEN, S.M. (2002): U–Pb geochronology of detrital zircons in metasedimentary rocks from southern Baffin Island: implications for the Paleoproterozoic tectonic evolution of northeastern Laurentia. *Can. J. Earth Sci.* **39**, 611-623.

SEYDOUX-GUILLAUME, A.-M., PAQUETTE, J.-L., WIEDENBECK, M., MONTEL, J.-M. & HEINRICH, W. (2002): Experimental resetting of the U–Th–Pb systems in monazite. *In* Chemistry and Physics of Accessory Minerals: Crystallisation, Transformation and Geochronological Applications. *Chem. Geol.* **191**, 165-181.

SIDDORN, J.P. & HALLS, H.C. (2002): Variation in plagioclase clouding intensity in Matachewan dykes: evidence for the exhumation history of the northern margin of the Sudbury igneous complex. *Can. J. Earth Sci.* **39**, 933-942.

SKULSKI, T., SANBORN-BARRIE, M. & SANDEMAN, H. (2003b): Geology, Walker Lake and Arrowsmith River area, Nunavut. *Geol. Surv. Can., Open File* **3777** (1:100,000 scale, 2 sheets).

________, SANDEMAN, H., SANBORN-BARRIE, M., MACHATTIE, T., HYDE, D., JOHNSTONE, S., PANAGAPKO, D. & BYRNE, D. (2002a): Contrasting crustal domains in the Committee Bay belt, Walker Lake–Arrowsmith River area, central Nunavut. *Geol. Surv. Can., Curr. Res.* **2002–C11**, 1-10.

________, ________, ________, ________, YOUNG, M., CARSON, C., BERMAN, R.G., BROWN, J., RAYNER, N., PANAGAPKO, D., BYRNE, D. & DEYELL, C. (2003a): Bedrock geology of the Ellice Hills map area and new constraints on the regional geology of the Committee Bay area, Nunavut. *Geol. Surv. Can., Curr. Res.* **2003–C22**, 1-11.

________, ________, ________, RAYNER, N. & KISS, F. (2002b): New geological, geophysical and geochronological constraints on the evolution of the Committee Bay belt, central Nunavut. *Geol. Assoc. Can. – Mineral. Assoc. Can., Program Abstr.* **27**, 110.

SPEAR, F.S. (1993): *Metamorphic Phase Equilibria and Pressure – Temperature – Time Paths*. Mineralogical Society of America, Washington, D.C.

________ & DANIEL, C.G. (2003): Three-dimensional imaging of garnet porphyroblast sizes and chemical zoning; nucleation and growth history in the garnet zone. *Am. Mineral.* **88**, 245.

STERN, R.A. & BERMAN, R.G. (2000): Monazite U–Pb and Th–Pb geochronology by ion microprobe, with an application to *in situ* dating of an Archean metasedimentary rock. *Chem. Geol.* **172**, 113–130.

STOCKWELL, C.H. (1982): Proposals for time classification and correlation of Precambrian rocks and events in Canada and adjacent areas of the Canadian Shield. I. A time classification of Precambrian rocks and events. *Geol. Surv. Can., Pap.* **80–19**.

ST-ONGE, M.R., SCOTT, D.J. & WODICKA, N. (2002): Review of crustal architecture and evolution in the Ungava Peninsula – Baffin Island area: connection to the Lithoprobe ECSOOT transect. *Can. J. Earth Sci.* **39**, 589-610.

STOWELL, H.H. & GOLDBERG, S.A. (1997): Sm–Nd garnet dating of polyphase metamorphism: northern Coast Mountains, south-eastern Alaska, USA. *J. Metamorph. Geol.* **15**, 439-450.

SUZUKI, K. & ADACHI, M. (1991): Precambrian provenance and Silurian metamorphism of the Tsubonosawa Paragneiss in the South Kitakami Terrane, northeast Japan, revealed by the chemical Th–U–total Pb isochron ages of monazite, zircon and xenotime. *Geol. J.* **25**, 357-376.

________, ________ & Kajizuka, I. (1994): Electron microprobe observations of Pb diffusion in metamorphosed detrital monazites. *Earth Planet. Sci. Lett.* **128**, 391-405.

Tella, S., Davis, W., Berman, R.G., Stern, R. & LeCheminant, A.N. (1997): Tectonothermal history of the MacQuoid Lake supracrustal belt, District of Keewatin, Northwest Territories, Canada. *Geol. Soc. Am., Abstr. Program* **29**, 277-278.

________ & Heywood, W.W. (1978): The structural history of the Amer mylonite zone, Churchill structural province, District of Keewatin. *Geol. Surv. Can., Curr. Res.* **78–1C**, 79-88.

Thériault, R.J. (1992): Nd isotopic evolution of the Taltson magmatic zone, Northwest Territories, Canada; insights into early Proterozoic accretion along the western margin of the Churchill Province. *J. Geol.* **100**, 465-475.

________, Henderson, J.B. & Roscoe, S.M. (1994): Nd isotopic evidence for early to mid-Archean crust from high grade gneisses in the Queen Maud Block and south of the McDonald Fault, western Churchill Province, Northwest Territories. *In* Radiogenic Age and Isotopic Studies. Report 8. *Geol. Surv. Can., Curr. Res.* **1994–F**, 37-42.

________, St-Onge, M.R. & Scott, D.J. (2001): Nd isotopic and geochemical signature of the Paleoproterozoic Trans-Hudson Orogen, southern Baffin Island, Canada: implications for the evolution of eastern Laurentia. *Precamb. Res.* **108**, 113-138.

Thompson, P. (1998): Regional geological setting of gold occurrences in the southwestern segment Committee Bay Belt, south-central Nunavut. Internal report for Committee Bay Joint Venture on behalf of Committee Bay Resources Ltd., 66 p. (4 maps, 1:250,000 scale).

Tinkham, D.K., Zuluaga, C.A. & Stowell, H.H. (2003): Metapelite phase equilibria modeling in MnNCKFMASH: the effect of variable Al_2O_3 and MgO/(MgO + FeO) on mineral stability. *Am. Mineral.* **88**, 1174.

Tran, H.T., Ansdell, K., Bethune, K., Watters, B. & Ashton, K. (2003): Nd isotope and geochemical constraints on the depositional setting of Paleoproterozoic metasedimentary rocks along the margin of the Archean Hearne Craton, Saskatchewan, Canada. *Precamb. Res.* **123**, 1-28.

Tremblay, L.P., Loveridge, W.D. & Sullivan, R.W. (1981): U–Pb ages of zircons from the Foot Bay Gneiss and the Donaldson Lake Gneiss, Beaverlodge area, northern Saskatchewan. *Geol. Surv. Can., Curr. Res.* **81–1C**, 123-126.

Van Breemen, O., Bostock, H.H. & Loveridge, W.D. (1992): Geochronology of granites along the margin of the northern Taltson Magmatic Zone and western Rae Province, Northwest Territories. *In* Radiometric Age and Isotopic Studies. Report 5. *Geol. Surv. Can., Curr. Res.* **91–2**, 17-24.

Van Schmus, W.R., Persons, S.S., MacDonald, R., Sibbald, T.I.I., Patterson, D.F. & Davie, R.F. (1986): Preliminary results from U–Pb zircon geochronology of the Uranium City region, northwest Saskatchewan. *Saskatchewan Geol. Surv., Summary of Investigations* **86–4**, 108-111.

Vance, D. & Harris, N. (1999): Timing of prograde metamorphism in the Zanskar Himalaya. *Geology* **27**, 395-398.

________, Meier, M. & Oberli, F. (1998a): The influence of high U–Th inclusions on the U–Th–Pb systematics of almandine–pyrope garnet: results of a combined bulk dissolution, stepwise-leaching, and SEM study. *Geochim. Cosmochim. Acta* **62**, 3527-3540.

________ & O'Nions, R.K. (1990): Isotopic chronometry of zoned garnets; growth kinetics and metamorphic histories. *Earth Planet. Sci. Lett.* **97**, 227-240.

________ & ________ (1992): Prograde and retrograde thermal histories from the central Swiss Alps. *Earth Planet. Sci. Lett.* **114**, 113-129.

________, Strachan, R.A. & Jones, K.A. (1998b): Extensional versus compressional settings for metamorphism; garnet chronometry and pressure – temperature – time histories in the Moine Supergroup, northwest Scotland. *Geology* **26**, 927-930.

Villeneuve, M.E., Ross, G.M., Thériault, R.J., Miles, W., Parrish, R. & Broome, J. (1993): Tectonic subdivision and U–Pb geochronology of the crystalline basement of the Alberta basin, western Canada. *Geol. Surv. Can., Bull.* **447**.

Williams, M.L. & Jercinovic, M.J. (2002): Microprobe monazite geochronology: putting absolute time into microstructural analysis. *In* Microstructural Processes: a Special Issue in Honor of the Career Contributions of R. H. Vernon. *J. Struct. Geol.* **24**, 1013-1028.

________, ________ & Terry, M.P. (1999): Age mapping and dating of monazite on the electron microprobe; deconvoluting multistage tectonic histories. *Geology* **27**, 1023-1026.

Wing, B.A., Ferry, J.M. & Harrison, T.M. (2003): Prograde destruction and formation of monazite and allanite during contact and regional metamorphism of pelites: petrology and geochronology. *Contrib. Mineral. Petrol.* **145**, 228-250.

Wodicka, N., St-Onge, M.R., Scott, D.J. & Corrigan, D. (2003): Age and provenance of the Piling Group, central Baffin Island, Nunavut. *Mineral Exploration Roundup 2004, Vancouver, B.C.*

Zhou, Bo & Hensen, B.J. (1995): Inherited Sm/Nd isotope components preserved in monazite inclusions within garnets in leucogneiss from East Antarctica and implications for closure temperature studies. *Chem. Geol.* **121**, 317-326.

Zhu, Z.K., O'Nions, R.K., Belshaw, N.S. & Gibb, A.J. (1997): Lewisian crustal history from *in situ* SIMS mineral chronometry and related metamorphic textures. *Chem. Geol.* **136**, 205-218.

Received December 18, 2003, revised manuscript accepted December 20, 2004.